AD-A144 872 COMPARISON OF THE HOLLOW CYLINDER AND THE TRULY TRIAXIAL TEST APPARATUSES..(U) COLORADO UNIV AT BOULDER DEPT OF CIVIL ENVIRONMENTAL AND ARCH.. F R SMITH 1983 1/1

UNCLASSIFIED N66314-70-A-0062 F/G 8/13 NL

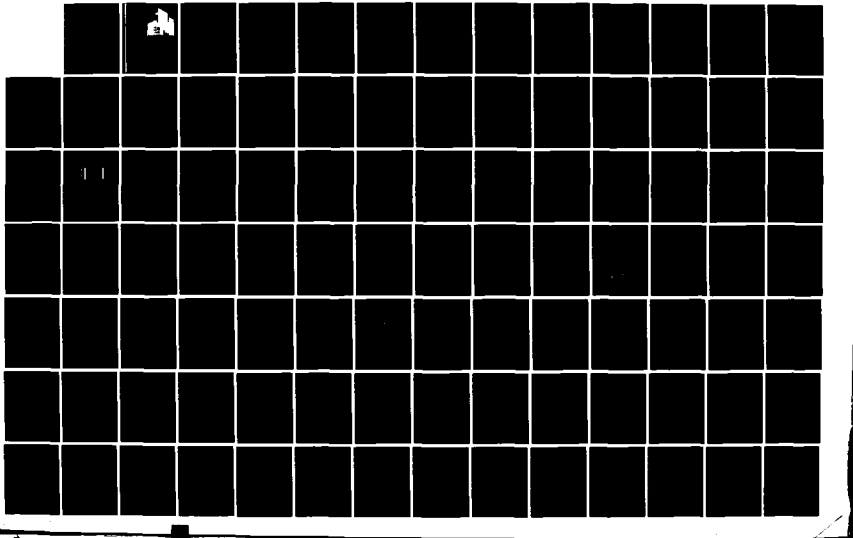

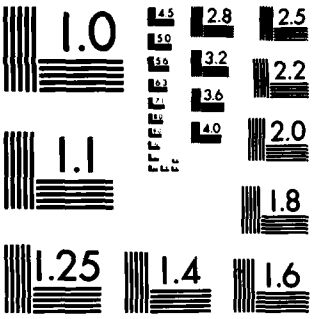

MICROCOPY RESOLUTION TEST CHART
NATIONAL BUREAU OF STANDARDS-1963-A

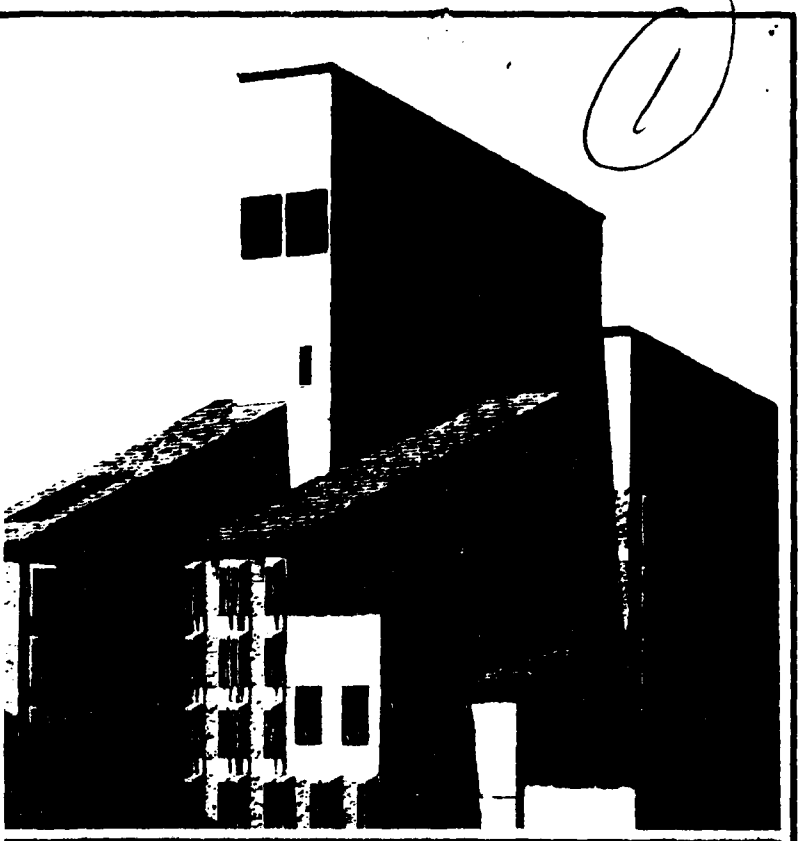

COMPARISON OF THE HOLLOW CYLINDER AND THE TRULY TRIAXIAL TEST APPARATUSES FOR THE STUDY OF ANISOTROPIC CLAYS

by

Frederick R. Smith

Department of Civil, Environmental, and Architectural Engineering

University of Colorado, Boulder
Box 428
Boulder, CO 80309

COMPARISON OF THE HOLLOW CYLINDER AND THE TRULY TRIAXIAL TEST APPARATUSES FOR THE STUDY OF ANISOTROPIC CLAYS

by

Frederick R. Smith

COMPARISON OF THE HOLLOW CYLINDER AND THE TRULY TRIAXIAL TEST APPARATUSES FOR THE STUDY OF ANISOTROPIC CLAYS

by

Frederick R. Smith

B.S., University of Delaware, 1978

A report submitted to the

Faculty of the Graduate School of the

University of Colorado in partial fulfillment

of the requirements for the degree of

Master of Science

Department of Civil, Environmental,

and Architectural Engineering

1983

A-1

This Report for the Master of Science Degree by

Frederick R. Smith

has been approved for the

Department of Civil, Environmental,

and Architectural Engineering

by

_____

Hon-Yim Ko

_____

Stein Sture

_____

Bernard Amadei

Date _____

TABLE OF CONTENTS

LIST OF FIGURES

Figure

LIST OF TABLES

CHAPTER I

INTRODUCTION

It is widely recognized that naturally deposited clays are anisotropic and that their behaviors, in addition to other factors, stress path dependent. Therefore, the degree of success in predicting the in situ strength and deformation behavior from laboratory test data lies in the ability to realistically model the inherently three-dimensional stress path conditions expected to be encountered in the field. Two testing devices which are capable of systematically and independently controlling the magnitude and direction of the three principal stresses are the hollow cylinder apparatus and the truly triaxial apparatus.

The primary purpose of this report is to discuss the advantages and the disadvantages of the hollow cylinder apparatus and the truly triaxial apparatus under static loading conditions. Particular attention is drawn to their capability for investigation of the anisotropy, strength, and deformation behavior of natural, undisturbed clays under undrained conditions.

Selected laboratory test results of anisotropic undrained strength behavior are presented and explained on the basis of the structural arrangement of individual clay particles and fabric units in the shear zone.

Background

Natural clays as they occur in situ, as well as man-made fills, are ideally deposited and consolidated in horizontal layers where no lateral straining occurs. Under such conditions the ratio of lateral to vertical stresses is known as the coefficient of earth pressure at rest, and is denoted by the symbol K_o. Electron microscope studies of clay particle orientation by Mitchell, Martin, and Roseqvist (17) leave no doubt that the non-symmetrical, plate like shape of the clay sized particles causes them to respond in a sensitive way to the directional bias of the initial deposition, K_o-consolidation, and subsequent application of stresses.

Anisotropic K_o-consolidation, that is where K_o is not equal to unity, imposes what researchers term stress-induced cross or transverse anisotropy. Cross anisotropy results from the tendency of the clay particles to become oriented normal to the direction of the major principal stress; e.g., the vertical stress for the general in situ condition where K_o is a value less than one. The direction of consolidation, which is generally parallel to the vertical axis of the deposit, as illustrated in Figure 1, is the direction of the axis of rotational symmetry.

The undrained strength and other mechanical properties of clay soils are governed to a large extent by the clay soil structure, which consists of the complex combination of particle arrangements termed fabric and interparticle bonds. It is the

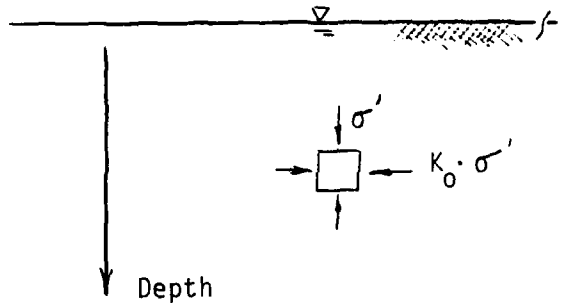

Figure 1. Normally Consolidated Clay Deposit

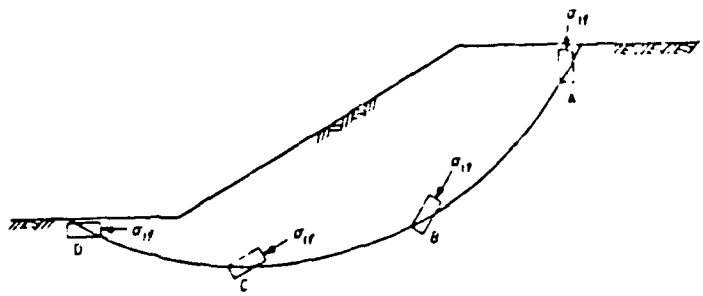

Figure 2. Orientation of Stress Directions at Failure

soil structure which provides the integrity of the system, and which is responsible for response to externally applied sets of forces. Consequently, following the observation that natural clays as they occur in situ are cross anisotropic relative to the fabric component of structure, there must be a direction-dependence of the undrained stress-strain response which is fundamentally related to the soil fabric.

The degree of success in predicting the in situ strength and deformation behavior of soils from laboratory test data lies in the ability to realistically model the varied stress path conditions expected to be encountered in the field. To illustrate the stress paths associated with most field loading and unloading problems, Figure 2 shows the same clay deposit as Figure 1 after excavation of a cut. Geotechnical analyses and comparisons with field cases indicate that the circular arc failure surface ABCD, approximates the actual failure (8). The orientations of the major principal stress at incipient failure are shown at points A, B, C, and D. If the major principal stress at the time of consolidation was vertical, it can be seen that the degree of reorientation of the major principal stress along the failure surface varies from essentially zero at point A, to a maximum of 90° at point D.

The undrained stress-strain response of an element in a natural clay deposit to changes in the magnitude and direction of the principal stresses will be anisotropic, and will reflect

the geometrical arrangement of the clay particles and their contact. Laboratory equipment used to study and predict anisotropic soil behavior under load must be able to control and measure the magnitudes and directions of the three principal stresses and strains; that is, the equipment must be able to simulate the conditions expected to be encountered in the field.

The following chapters of this report review and evaluate the advantages and limitations of the hollow cylinder apparatus and the truly triaxial apparatus, both with which anisotropy, strength, and deformation behavior can be investigated. The capabilities of these devices are judged for static loading conditions according to the following general criteria:

(1) Can the device apply uniform states of stress and measure stress-strain response?

(2) Can the device systematically vary the magnitudes and the direction of all three principal stresses?

(3) Can the device be used to measure stress-strain-strength anisotropy?

CHAPTER II

HOLLOW CYLINDER APPARATUSES

Stress Application in the Hollow Cylinder Apparatus

The hollow cylinder apparatus is designed and constructed to permit application of internal and external confining pressures to a hollow cylinder specimen. Torsional shear and vertical stresses can be applied to the top end of the cylinder while the bottom end platten remains stationary. The general layout of a hollow cylinder apparatus used at Imperial College, London is shown in Figure 3 (10).

In principle, normal and shear stresses are applied to the specimen according to the following technique. The confining pressures of the inner and outer cell, which may or may not be equal, are applied through the cell fluid and are transmitted to the specimen through flexible membranes. The vertical load is applied to the specimen by the top end platten which is also acted on by the cell pressures. The torque is transferred to the specimen by adhesion between the top end platten and the specimen. The shear stresses due to torque cause reorientation of the principal stress directions and a stress field with three unequal principal stresses.

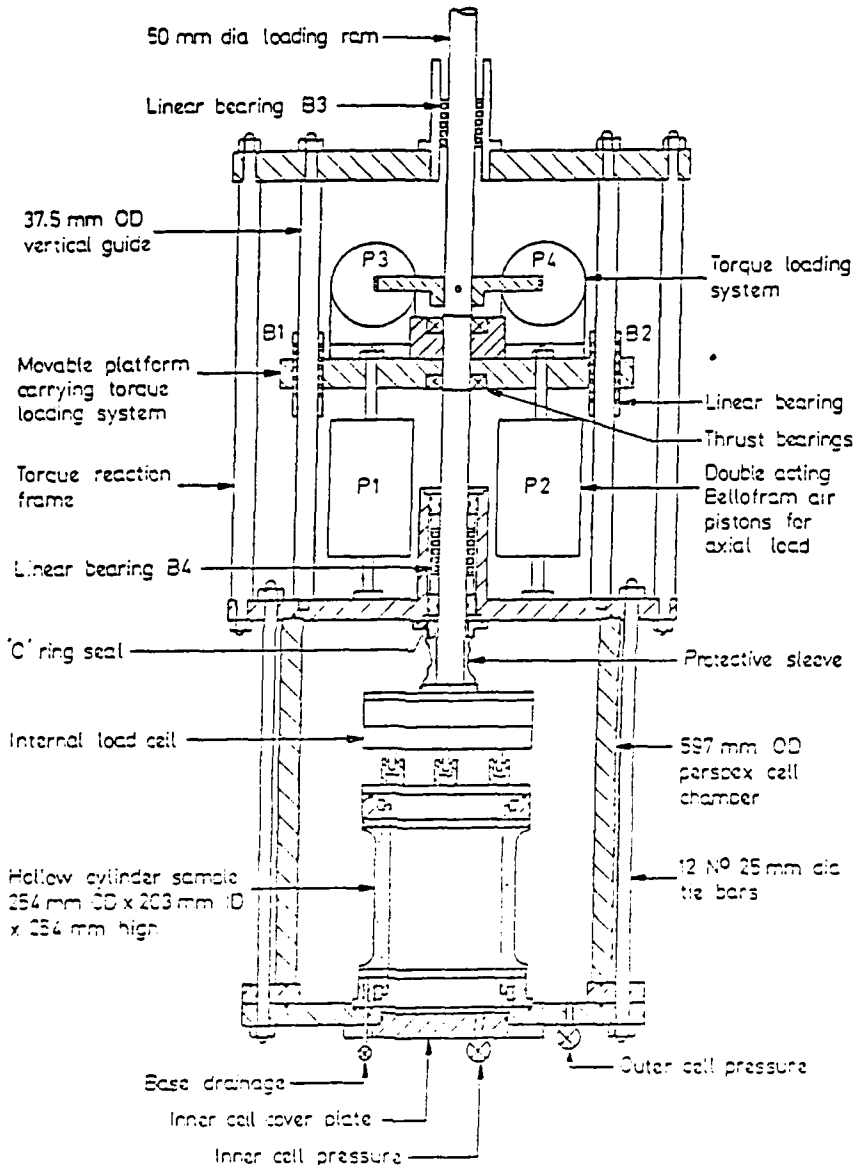

Figure 3. General Layout of the Hollow Cylinder Apparatus (10)

Stress Distributions in the Hollow Cylinder Specimen

The stresses which act on the wall of a hollow cylinder specimen subjected to a combination of axial, torsional and spherical stresses are shown in Figure 4. The torque, M_t, develops shear stresses $\tau_{\theta z}$ and $\tau_{z\theta}$, in vertical and horizontal planes; the axial load, W, contributes to a vertical stress, σ_z; and the difference between the internal and external pressures, P_i and P_o respectively, establish a gradient of radial stress, σ_r, and circumferential stress, σ_θ, across the cylinder wall. If the effects of end restraint are neglected (the validity of which will be discussed) there are no shear stresses on circumferential surfaces throughout the wall and the radial stress, σ_r, is always a principal stress. The remaining acting stresses may be resolved to determine the magnitude and the direction of the other two principal stresses which will always lie in the vertical plane of the specimen. Thus, rotation is restricted to one plane.

In principle, the hollow cylinder apparatus appears to be a tool which allows investigators unrestricted exploration of stress space, including rotation of the principal stresses. There are, however, shortcomings in the use of the hollow cylinder apparatus. Stress and hence strain nonuniformities develop in the wall of the specimen as a result of:

(1) curvature of the wall, and

(2) end restraint.

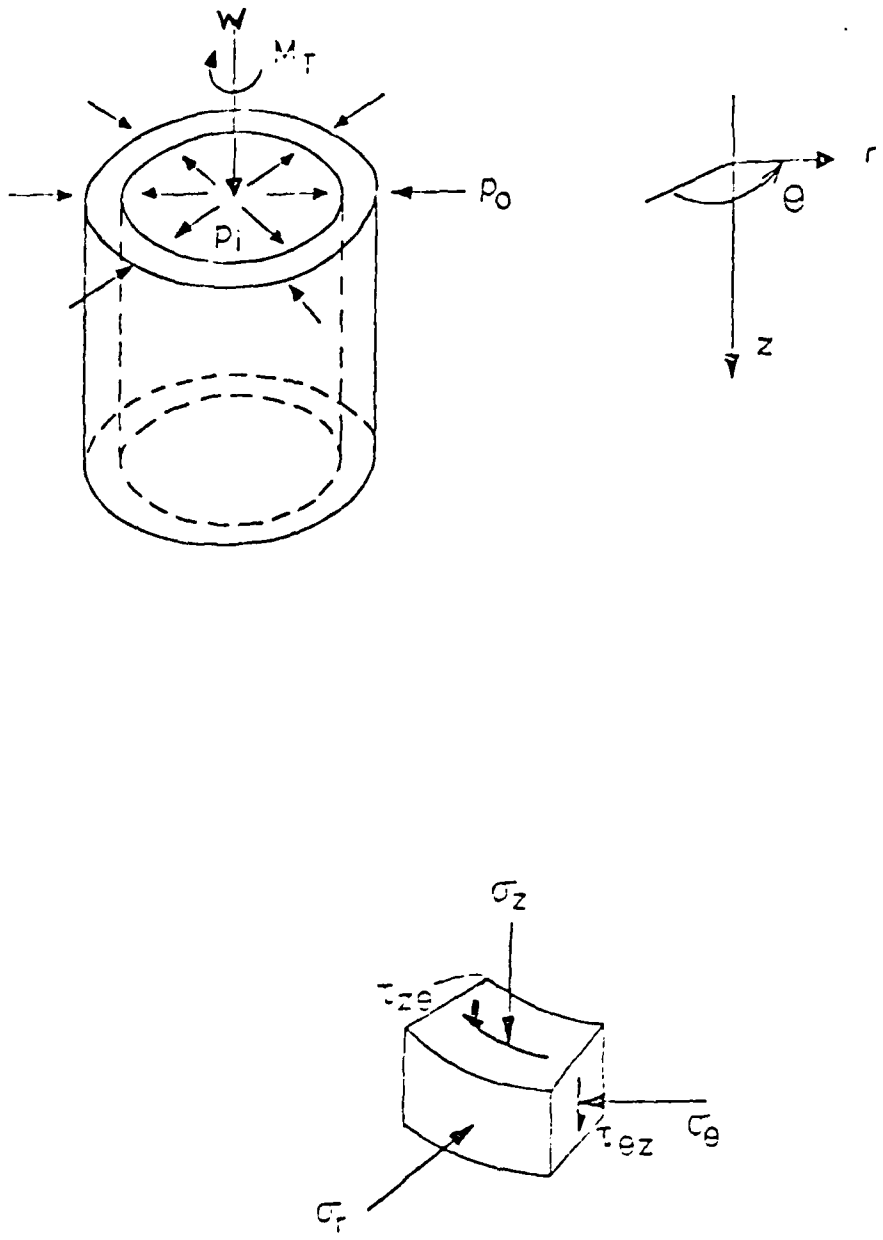

Figure 4. Stresses in the Hollow Cylinder Specimen

Stress nonuniformity due to curvature arises when a torque or a difference in the internal and external pressures are applied. Torque leads to a variation in shear stress, $\tau_{\theta z}$, across the wall, which causes nonuniformities in σ_z, σ_r, and σ_θ. As previously mentioned, differences in internal and external cell pressures give rise to a gradient of σ_r and σ_θ across the wall. The magnitudes of these nonuniformities are dependent on sample geometry, on the stress path to be followed, and on the specimen's constitutive relations. Nonuniformities can be minimized by careful selection of the wall thickness and the inner and outer radii, nevertheless, regions exist in stress space where the required cell pressure difference and the resulting stress gradient become unacceptably large. This will be discussed in the following section on the interpretation of stress and strain distributions in the hollow cylinder specimen.

Stress nonuniformities arising from end restraint are introduced by the frictional restraint and stiffness of the end plattens. These nonuniformities are in addition to those arising from the specimen's curvature. Restraint on radial displacement of the specimen, which is the case if the specimen has a tendency to expand or contract, results in the development of radial shear stresses whose magnitude is dependent on sample geometry, the specimen's constitutive properties, and the applied pressure and load combinations. The radial shear,

τ_{zr} and its conjugate τ_{rz}, vanish as the distance away from the end plattens increases. St. Venant's principle of rapid dissipation of localized stresses applies at a certain minimum distance from the end plattens. Selection of sample height should be based upon consideration of St. Venant's principle and the need to provide an adequate central gage length in which stresses and strains are sufficiently uniform. Linear-elastic and separate plastic analyses by Hight et al (10) demonstrated that reasonably uniform distributions of stress differing by no more than 10% from those in an unrestrained specimen could be obtained with a suitably tall specimen, at least over a central gage length. The analyses also demonstrated that stress nonuniformities became larger as failure was approached, and that higher levels of nonuniformities are associated with drained loading (Poisson's ratio less than 0.49).

Using the theory of elasticity or plasticity applied to fixed end cylindrical shells, it is possible to study the stress distributions in specimens of different geometry. The literature is in agreement that the effect of stress nonuniformities can then be reduced to an acceptable level by judicious selection of the specimen geometry. A review of the geometries used by various researchers shows that there is obviously no agreement on an optimum geometry for general testing. Because different levels of nonuniformity are associated with different

geometries, conclusions drawn from the comparison of test data from the various apparatuses are suspect. It has been argued by Hight et al (10) that substantially more uniform stress distribution than previously thought possible can be achieved by using a specimen with inside and outside diameters of 203 mm (8.1 in) and 254 mm (10.0 in) respectively and a height of 254 mm (10.0 in).

Instrumentation for Monitoring Deformation and Rotation

An element in the wall of a specimen may deform radially, axially, and circumferentially. Instrumentation for measuring relative displacement between two points must consider these three components of movement which are illustrated in Figure 5. The monitoring of radial displacement, the change in the thickness of the specimen wall, can be accomplished by using pairs of proximity transducers measuring the radial displacements u_i and u_o, of the inner and outer surfaces of the cylinder wall as shown in Figure 6 (10). Vertical displacement, the change in height of the specimen denoted by the symbol w, is either measured outside the cell using displacement transducers mounted on the loading ram and in contact with the cell top or preferably with pairs of electrolevel devices mounted on the surface of the cylinder wall. The combination of the two surface mounted electrolevels shown in Figure 7 provides a measure of both the vertical and circumferential displacement (10). The circumferential displacement, v, can also be

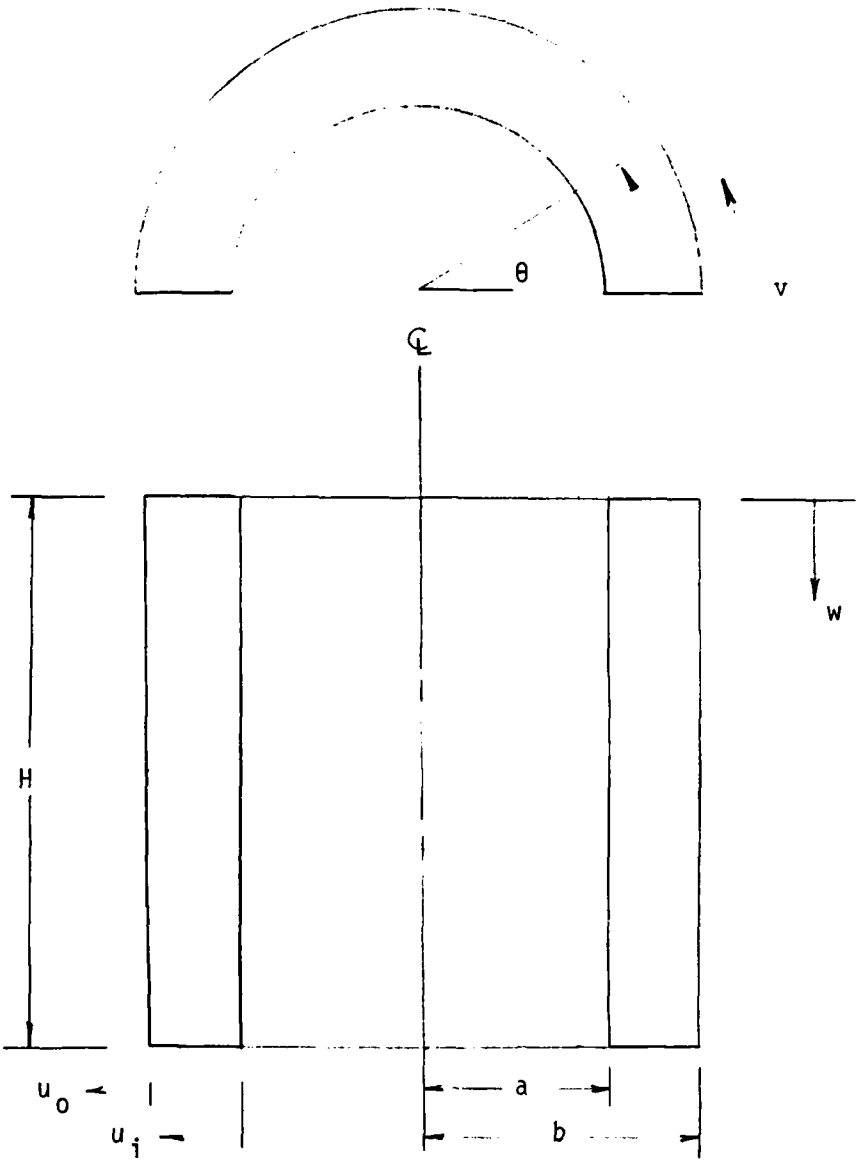

u_o, u_i } radial displacement

w : vertical displacement

θ : angular circumferential distortion

v : circumferential displacement

Figure 5. Components of Displacement

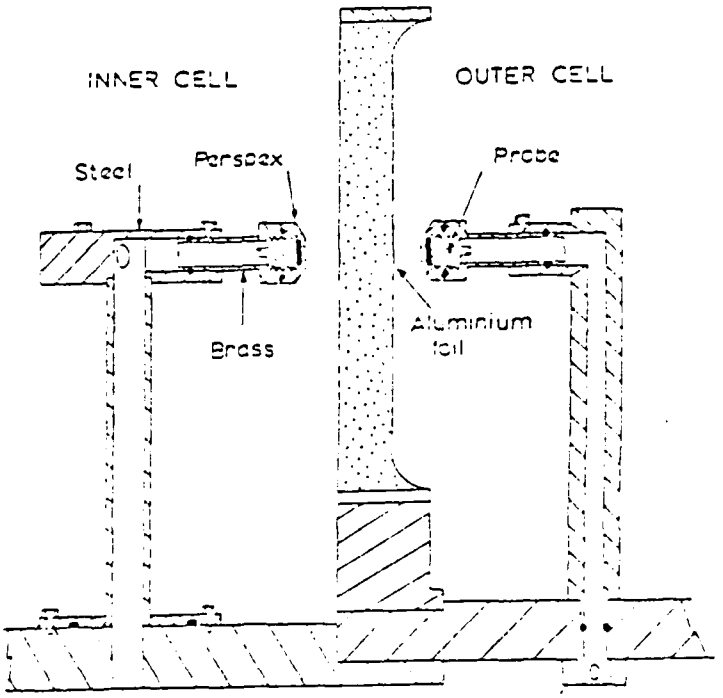

Figure 6. Instrumentation for Radial Displacement (10)

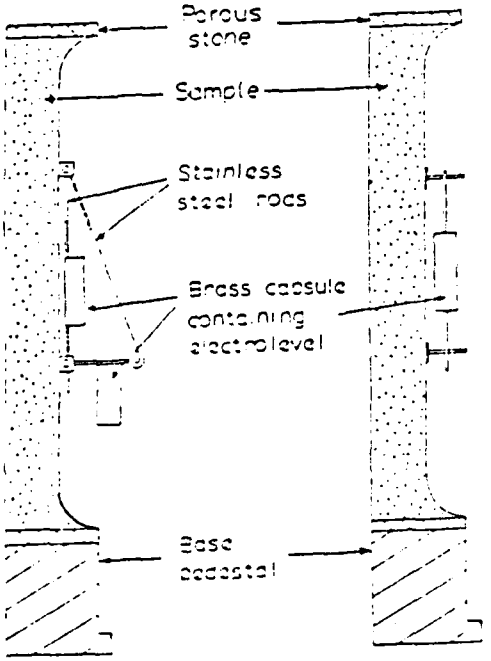

Figure 7. Instrumentation for Axial and Circumferential Displacement (10)

measured directly using a single, surface mounted electrolevel device. Angular circumferential distortion, θ, is measured outside the cell using a transducer mounted horizontally on the arm which is fixed to the loading ram and used to apply torque to the top of the cell.

If the cell is constructed of transparent materials, it offers the advantage of allowing direct observation of the specimen during the test. By inscribing a grid on the outer membrane, an overall view of the uniformity of deformation can be obtained using photogrammetry. Changes in the photographic pairs taken at intervals during the test can be resolved to vertical and circumferential displacements as a check against the internal instrumentation.

Interpretation of Stress and Strain Distributions

In view of the stress and strain nonuniformities, interpretation of tests in the hollow cylinder apparatus is made by considering the specimen as a single element and working in terms of average values for stress and strain. Since neither the principal stresses nor strains can be measured directly across the wall of the specimen, the average values must be calculated using the expressions given in Figure 8. Derivation of these formulas requires that the following assumptions be valid.

(1) No warping or bending normal to the axis of a specimen takes place.

Average vertical stress, $\bar{\sigma}_z = \frac{W}{\pi(b^2 - a^2)} + \frac{(p_o b^2 - p_i a^2)}{(b^2 - a^2)}$ (1)

Average radial stress, $\bar{\sigma}_r = \frac{(p_o\, b + p_i a)}{(b + a)}$ (2)

Average circumferential stress, $\bar{\sigma}_\theta = \frac{(p_o\, b - p_i a)}{(b - a)}$ (3)

Average shear stress, $\bar{\tau}_{\theta z} = \frac{3M_T}{2\pi(b^3 - a^3)}$ (4)

Average axial strain, $\bar{\varepsilon}_z = \frac{w}{H}$ (5)

Average radial strain, $\bar{\varepsilon}_r = -\frac{(u_o - u_i)}{(b - a)}$ (6)

Average circumferential strain, $\bar{\varepsilon}_\theta = -\frac{(u_o + u_i)}{b + a)}$ (7)

Average shear strain, $\bar{\gamma}_{\theta z} = \frac{2.\theta(b^3 - a^3)}{3.H(b^2 - a^2)}$ (8)

Figure 8. Definitions of Average Stresses and Strains (10)

(2) The deformation due to applied torque is such that shearing strain, $\gamma_{\theta z}$, varies linearly from the longitudinal axis of the specimen. The basic assumption is that straight radial lines remain straight as shown in Figure 9.

(3) Deformations due to one force cause no change in the effect of another force. Hence, the resultant stress or strain in the specimen due to several forces is the algebraic sum of their effects when separately applied.

(4) The specimen is a thin walled cylinder for which the difference between a linear-elastic and plastic stress distribution is small regardless of the mechanical properties of the material. Therefore, the magnitude of the difference between the calculated and real stress or strain average is small.

The first three assumptions are difficult to directly justify, however, unquestionable validity has been demonstrated experimentally for the case of small shear strains (21). For angular circumferential distortions approaching and exceeding 10°, appreciable variations from the assumed deformation result. Also unacceptable warping and bending to the extent that the test results would be invalidated would be the result where the axis of symmetry of a cross anisotropic soil and the vertical axis of the specimen do not coincide. Although the testing of specimens trimmed obliquely to the principal material axes is not possible, the capability to rotate the principal stress

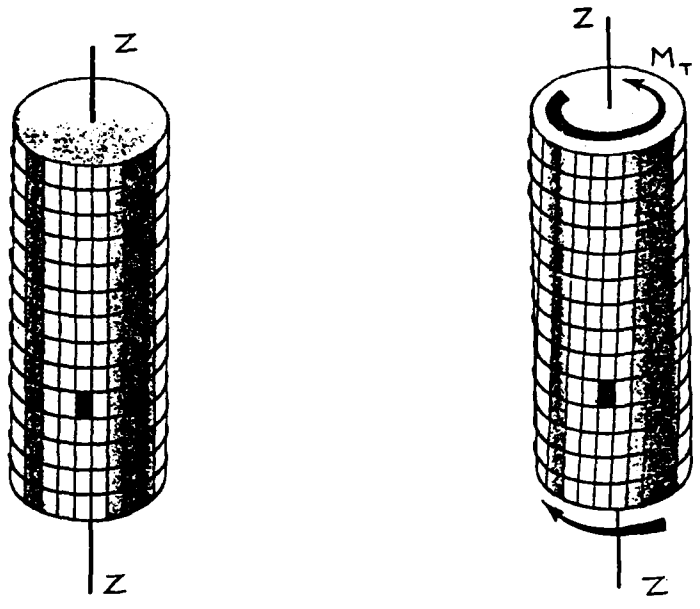

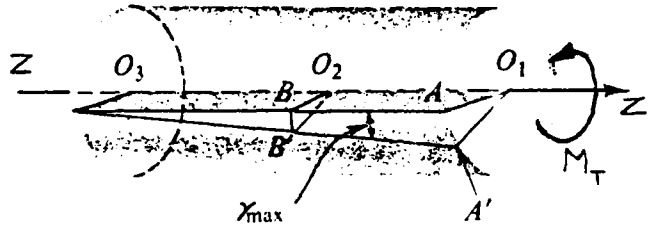

Figure 9. Assumed Deformation Due to Applied Torque (21)

direction makes that need nonexistent. A thin walled cylinder has been defined for engineering purposes as one having a wall thickness on the order of 10% of the radius or less. Few of the hollow cylinder apparatuses in use meet this requirement, in fact, most thicknesses are on the order of 20% of the radius. Therefore, calculated average values of stress and strain across the wall of the specimen may differ appreciably from the real averages. Practically speaking, the wall thickness is most governed by the need to insure a thickness which is large in relation to the potential thickness of the disturbed zone. The wall must also be substantial enough so as not to be subject to excess disturbance resulting from internal instrumentation for monitoring displacement and pore pressures.

The above assumptions are the basis for the derivations of the formulas in Figure 8. The average values for the vertical and circumferential stresses, $\bar{\sigma}_z$ and $\bar{\sigma}_\theta$ respectively, are based on equations of static equilibrium. The average axial and shear strains $\bar{\varepsilon}_z$ and $\bar{\gamma}_{\theta z}$, are based on strain compatibility for the assumed deformation. The expressions used for the remaining averages of stress are based on the assumption that the cylinder is thin walled. The formula for $\bar{\sigma}_r$ assumes a linear-elastic stress distribution, and that for $\bar{\tau}_{\theta z}$ assumes a uniform stress distribution. The expressions for average radial strains across the specimen wall, $\bar{\varepsilon}_r$ and $\bar{\varepsilon}_\theta$, assume a linear variation of strain.

To illustrate the link between stress combinations and stress nonuniformities arising from curvature for a selected geometry and wall thickness, bounds for P_o/P_i have been set at 1.2 and 0.9; these values lead to a maximum relative difference between the calculated average and real stresses of 11% (10). Stress states attainable within these bounds have been established for the orientation, β, of the major principal stress with respect to the specimen's vertical axis. The attainable stress states for values of $\beta = 0°, 45°$, and $90°$ are shown in the deviatoric plane in Figures 10 and 11. By comparing the two figures, it is apparent that the stress state limitations depend on the direction of the major principal stress. For $\beta = 0°$, larger differences between the inner and outer cell pressures are necessary to vary the magnitudes of the intermediate and minor principal stress. Consequently, the regions which can be investigated are severely restricted in comparison to the attainable stress states when $\beta = 45°$. For $\beta = 0°$, the boundaries to the attainable region narrow and approach the σ_I/σ_m axis. This restriction arises from the design of the apparatus whereby the inner and outer cell pressures contribute to both the horizontal and axial load. As P_i is decreased or P_o is increased the axial stress increases, however, stress nonuniformities quickly develop across the wall of the specimen as the difference between the cell pressures increases. In Figure 10, it can be seen that in the regions where the major principal stress is

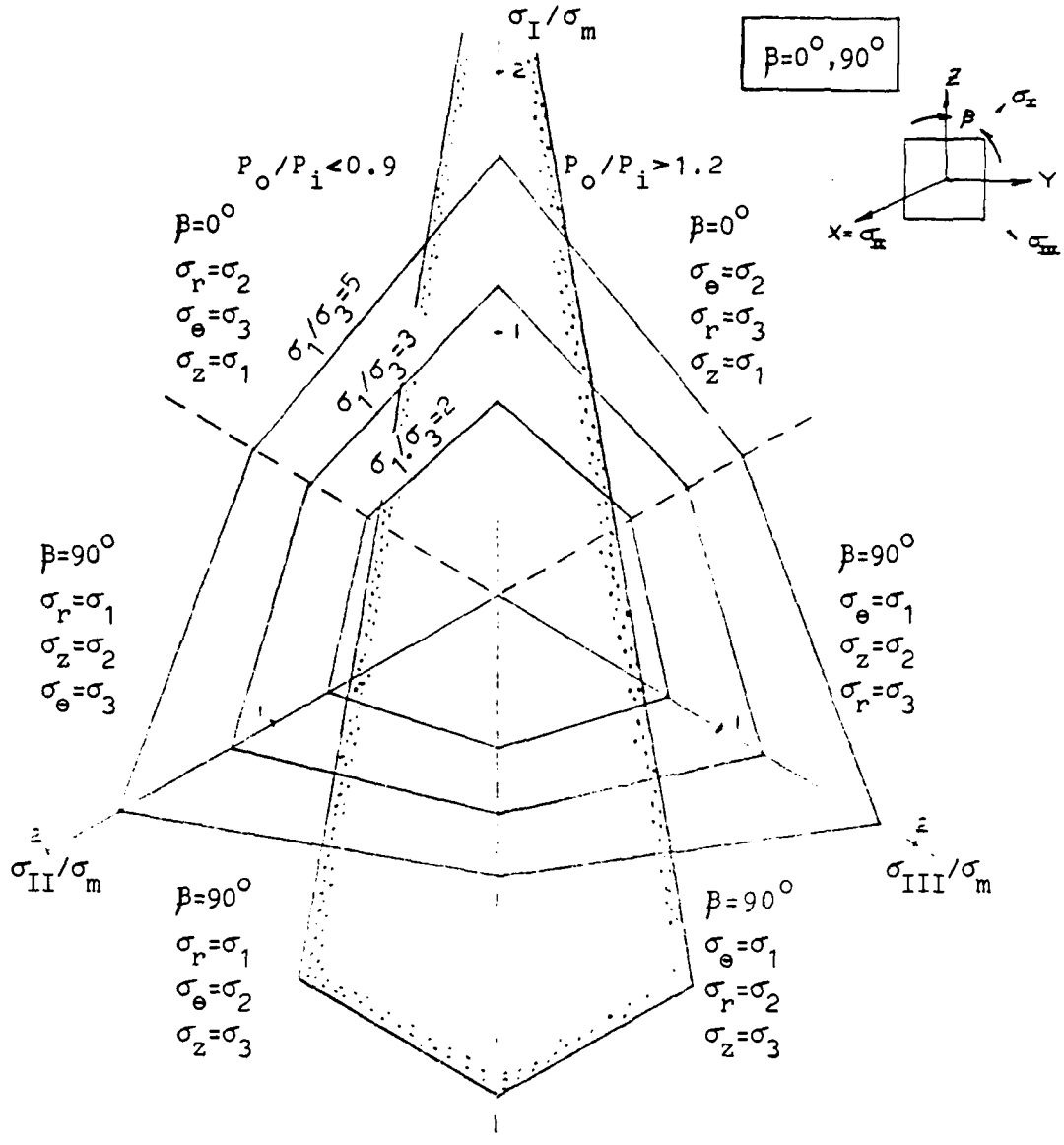

Boundary to the regions which can be investigated in the new hollow cylinder apparatus imposing the restriction that

$0.9 < P_o/P_i < 1.2$

σ_I, σ_{II}, σ_{III} are unordered principal stresses

σ_1, σ_2, σ_3 are ordered principal stresses

$\sigma_m = \frac{1}{3}(\sigma_1+\sigma_2+\sigma_3)$ the mean principal stress

Figure 10. Attainable Stress States (10)

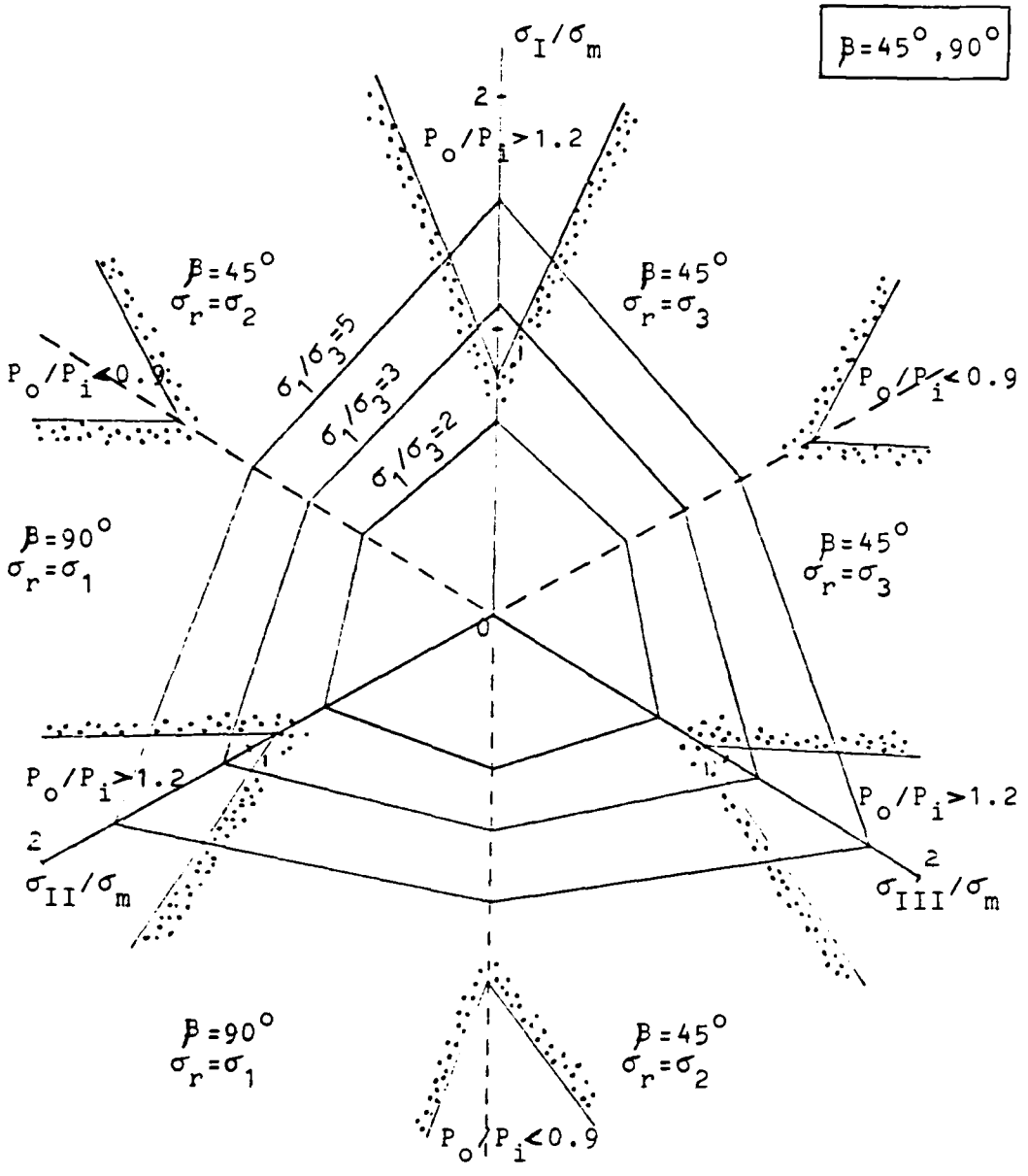

Figure 11. Attainable Stress States (10)

vertical, the maximum attainable value of σ_1/σ_3 may be as small as 2. This limitation prevents the testing of some highly plastic or stiff clays which may have values of $(\sigma_1/\sigma_3)_{max}$ exceeding 4. For $\beta = 90°$, achieved by requiring either of the horizontal stresses σ_r or σ_θ to be the major principal stress, the attainable region starts to open from the σ_I/σ_m axis until bound by the maximum working pressure of the apparatus. The greatest range of stress paths which can be investigated when $\beta = 90°$ occurs when the difference between σ_θ and σ_r is smallest; that is, when σ_z is the minor principal stress the nonuniformities in stress across the wall due to σ_r and σ_θ are minimized. Figure 11 shows that, when a torque is applied to rotate the principal stresses, σ_r remains a principal stress and that for a single value of applied torque two principal stress orientations can be achieved. For example, when σ_r is the major principal stress, then $\beta = 90°$, otherwise, $\beta = 45°$. Again, the more significant limitations are for states of compression when the major principal stress exceeds 2.5 times the minor stress. This arises because the maximum principal stress ratio at constant torque is a function of σ_z and σ_θ, whose magnitudes are directly dependent on the maximum difference which can be established between the inner and outer cell pressures.

The range of stress paths to be investigated should be selected on the basis of Figures 10 or 11, or a similar figure

which associates the expected degree of uniformity with the stress ratio to be investigated.

For the particular case of equal internal and external cell pressures, it is reasonable to assume that σ_r and σ_θ are uniform and equal to the applied cell pressure. The stress nonuniformities are minimized at the expense of flexibility in control. The following sections discussing the interpretation of stress distribution and data reduction will show that changes in $\tau_{\theta z}$, σ_z, σ_θ, and σ_r produce changes in the magnitude and orientation of the major and minor principal stresses and simultaneous changes in the intermediate principal stress. If the pressures are constrained to be equal, then the stress states are confined to the surfaces shown in Figure 12. It has been shown by others that the parameter b, a dimensionless variable defined in Figure 12, and the orientation, β, of the major principal stress are related by the expression,

$$b = \sin^2\beta \tag{9}$$

and independent control of b and β can not be achieved (10, 27). For example, in order to maintain a constant orientation of $\beta = 60°$, the value of b must be kept equal to 0.75.

Data Reduction Procedure

For anisotropic materials, the principal strain axes will not be coincident (coaxial) with the principal stress axes. The exception to this rule is when the applied principal stress axes are aligned with the principal material axes. In

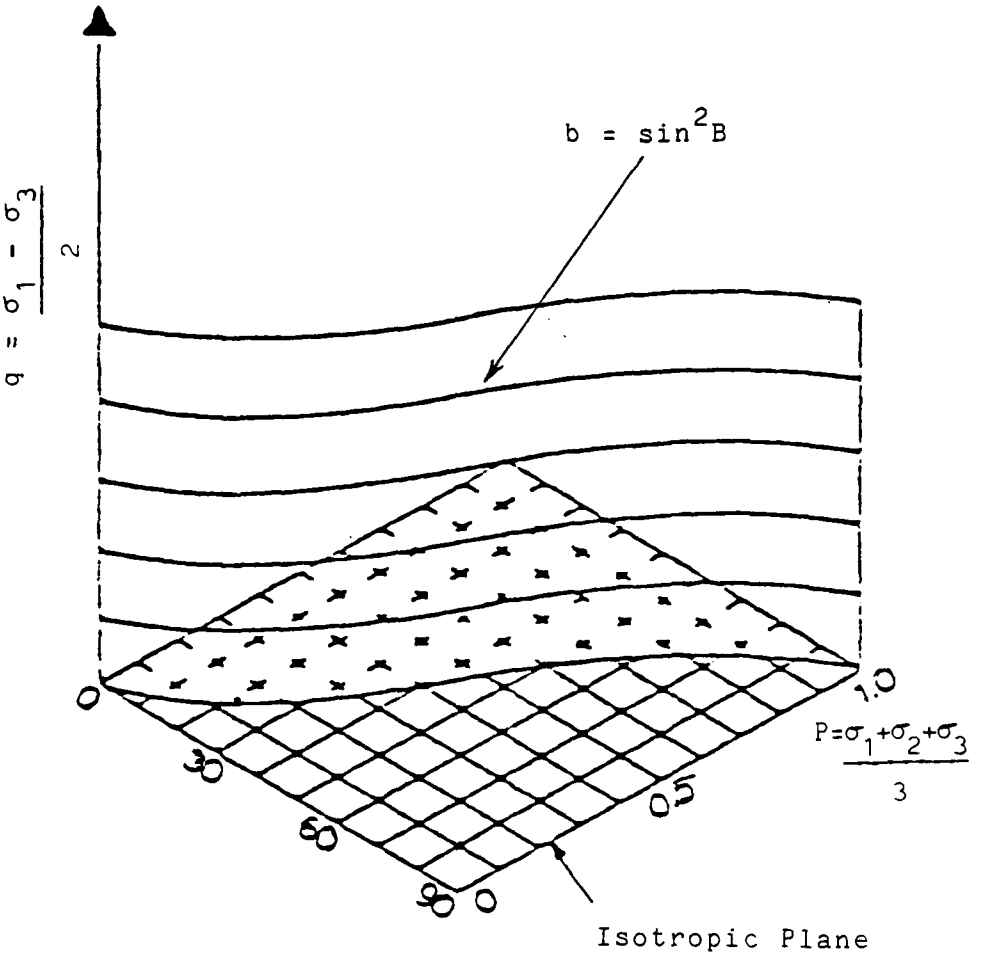

$$b = (\sigma_2 - \sigma_3)/(\sigma_1 - \sigma_3) \qquad (10)$$

Figure 12. Stress States for $P_o = P_i$ (34)

order to minimize bending and nonuniform distortion, the axes of the apparatus and the principal material axes must necessarily be coincident. Therefore, unless the principal stress axes and the axes of the apparatus are coincident, shear stresses and strains develop in the principal material planes and the principal stresses and strains will not be coincident. In order to relate the stresses to the strains, it is first necessary to express them in the same axes system. For the sake of clarity, the stresses and strains are ideally transformed to the XYZ principal material axes system to be defined in Figure 15. In the XYZ coordinate system, the Z axis is parallel to the axis of elastic symmetry. The X and Y axes lie in the plane of transverse isotropy. The stresses and strains expressed in the principal material axes system can then be related through Hooke's law for a linear-elastic material. The generalized Hooke's law can be represented in vector notation by,

$$\{\varepsilon_i\} = [C_{ij}]\ \{\sigma_i\} \qquad (11)$$

The strain and stress tensors, $\{\varepsilon_i\}$ and $\{\sigma_i\}$ respectively, are defined explicitly by a column arrangement of components. The tensor of compliances, $[C_{ij}]$ relating the stresses and strains is represented by a square array of components. Figure 13 shows the form of these tensors.

$$\left\{\epsilon_i\right\} = \begin{Bmatrix} \epsilon_1 \\ \epsilon_2 \\ \epsilon_3 \\ \epsilon_4 \\ \epsilon_5 \\ \epsilon_6 \end{Bmatrix} = \begin{Bmatrix} c_x \\ c_y \\ c_z \\ \gamma_{yz} \\ \gamma_{xz} \\ \gamma_{xy} \end{Bmatrix} \tag{12}$$

$$\left\{\sigma_i\right\} = \begin{Bmatrix} \sigma_1 \\ \sigma_2 \\ \sigma_3 \\ \sigma_4 \\ \sigma_5 \\ \sigma_6 \end{Bmatrix} = \begin{Bmatrix} \sigma_x \\ \sigma_y \\ \sigma_z \\ \sigma_{yz} \\ \sigma_{xz} \\ \sigma_{xy} \end{Bmatrix} \tag{13}$$

$$\left[C_{ij}\right] = \begin{bmatrix} C_{11} & C_{12} & C_{13} & C_{14} & C_{15} & C_{16} \\ C_{21} & C_{22} & C_{23} & C_{24} & C_{25} & C_{26} \\ C_{31} & C_{32} & C_{33} & C_{34} & C_{35} & C_{36} \\ C_{41} & C_{42} & C_{43} & C_{44} & C_{45} & C_{46} \\ C_{51} & C_{52} & C_{53} & C_{54} & C_{55} & C_{56} \\ C_{61} & C_{62} & C_{63} & C_{64} & C_{65} & C_{66} \end{bmatrix} \tag{14}$$

Figure 13. Definitions of $\left\{\epsilon_i\right\}$, $\left\{\sigma_i\right\}$ and $\left[C_{ij}\right]$

If the components of the compliance matrix are to be solved with respect to the principal material axes system, the magnitudes and directions of the applied stresses and measured strains must be calculated and rotated to the material axes system.

Using the formulas defined in Figure 14, the average stresses $\bar{\sigma}_z$, $\bar{\sigma}_r$, $\bar{\sigma}_\theta$, and $\bar{\tau}_{\theta z}$ can be resolved into average principal stresses $\bar{\sigma}_1'$, $\bar{\sigma}_2'$, and $\bar{\sigma}_3'$ at an angle β with respect to the material axes system. The ' denotes that the stresses are rotated with respect to the material axes system. Likewise, the average strains $\bar{\varepsilon}_z$, $\bar{\varepsilon}_\theta$, $\bar{\varepsilon}_r$, and $\bar{\gamma}_{\theta z}$ can be resolved into average principal strains $\bar{\varepsilon}_1'$, $\bar{\varepsilon}_2'$, and $\bar{\varepsilon}_3'$ at an angle α with respect to the material axes system. The principal stresses and strains can then be transformed, that is the principal axes of stress and strain can be rotated to the material axes system by a set of direction cosines between the axes systems. In the hollow cylinder apparatus, two of the principal stresses and two of the principal strains are always in the vertical plane, and the third principal stress and strain are always radial. Rotation is restricted to be in the vertical plane of the specimen. Thus, the rotated principal axes in the cartesian coordinate system where Z = Z, X = r, and Y = θ will be as shown in Figure 15. The orientation of the Z' and Y' axes with respect to the X, Y, and Z material axes can be

$$\bar{\sigma}'_I = \frac{\bar{\sigma}_z + \bar{\sigma}_\theta}{2} + \sqrt{\left(\frac{\bar{\sigma}_z - \bar{\sigma}_\theta}{2}\right)^2 + \bar{\tau}^2_{\theta z}} \quad (15)$$

$$\bar{\sigma}'_{II} = \frac{\bar{\sigma}_z + \bar{\sigma}_\theta}{2} - \sqrt{\left(\frac{\bar{\sigma}_z - \bar{\sigma}_\theta}{2}\right)^2 + \bar{\tau}^2_{\theta z}} \quad (16)$$

$$\bar{\sigma}'_{III} = \bar{\sigma}_r \quad (17)$$

$$\frac{1}{2}\tan 2\beta = \frac{\bar{\tau}_{\theta z}}{\bar{\sigma}_z - \bar{\sigma}_\theta} \quad (18)$$

$$\bar{\epsilon}'_I = \frac{\bar{\epsilon}_z + \bar{\epsilon}_\theta}{2} + \sqrt{\left(\frac{\bar{\epsilon}_z - \bar{\epsilon}_\theta}{2}\right)^2 + \left(\frac{\bar{\gamma}_{\theta z}}{2}\right)^2} \quad (19)$$

$$\bar{\epsilon}'_{II} = \frac{\bar{\epsilon}_z + \bar{\epsilon}_\theta}{2} - \sqrt{\left(\frac{\bar{\epsilon}_z - \bar{\epsilon}_\theta}{2}\right)^2 + \left(\frac{\bar{\gamma}_{\theta z}}{2}\right)^2} \quad (20)$$

$$\bar{\epsilon}'_{III} = \bar{\epsilon}_r \quad (21)$$

$$\frac{1}{2}\tan 2\alpha = \frac{\bar{\epsilon}_{\theta z}}{\bar{\epsilon}_z - \bar{\epsilon}_\theta} \quad (22)$$

$\bar{\sigma}'_I, \bar{\sigma}'_{II}, \bar{\sigma}'_{III}$ are unordered principal stresses oriented at angle β with respect to the material's axis of symmetry

$\bar{\epsilon}'_I, \bar{\epsilon}'_{II}, \bar{\epsilon}'_{III}$ are unordered principal strains oriented at angle α with respect to the material's axis of symmetry

Figure 14. Definitions of Average Principal Stresses and Strains

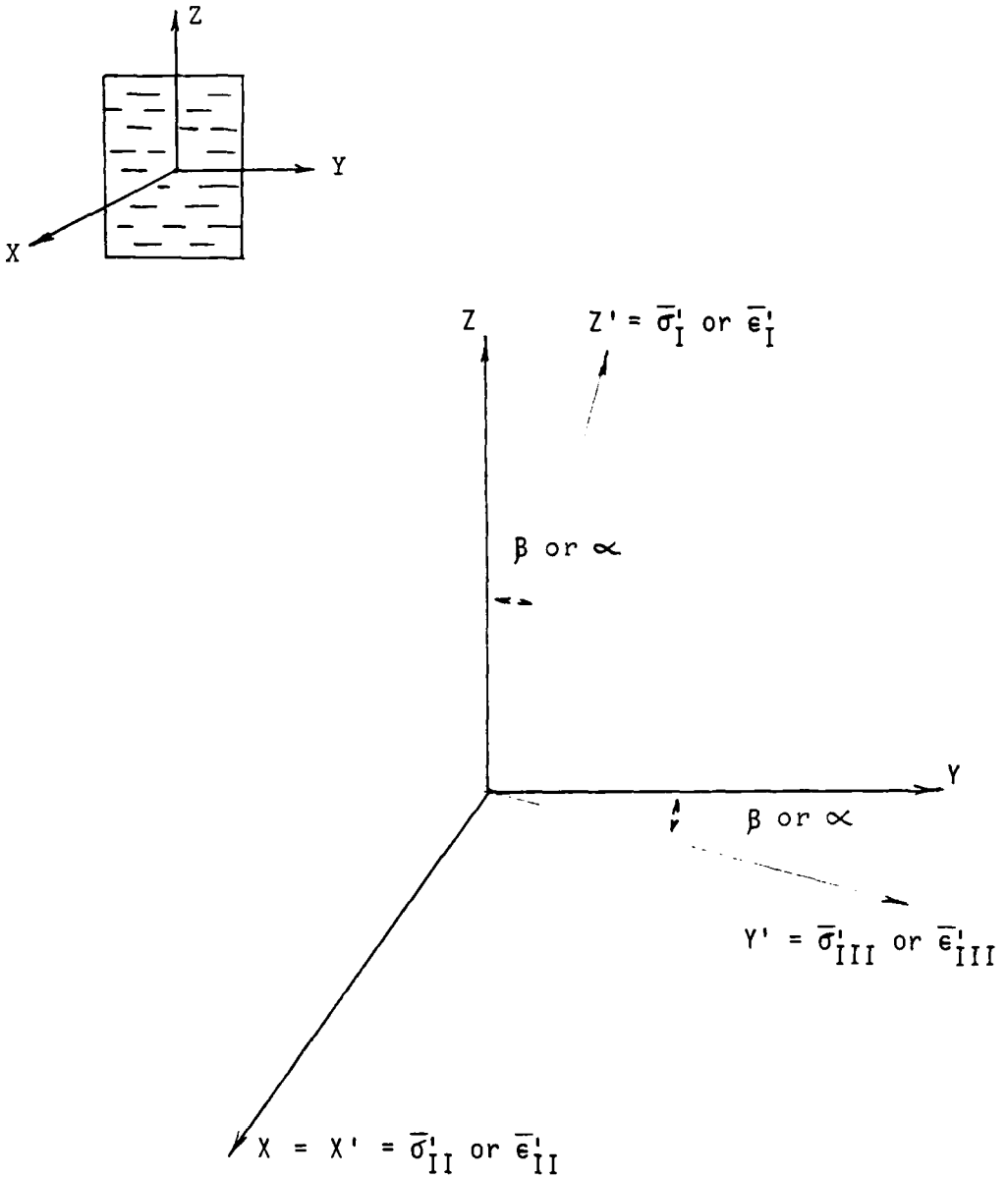

X,Y,Z: Material Axes System

X',Y',Z': Principal Stress or Strain Axes System

Figure 15. Rotation of Principal Axes

defined by one angle. The table of direction cosines between the principal axes system and the material axes can be written as,

TABLE 1

Direction Cosines

	X	Y	Z		X	Y	Z
σ_I'	0	$\sin\beta$	$\cos\beta$	ε_I'	0	$\sin\alpha$	$\cos\alpha$
σ_{II}'	1	0	0	ε_{II}'	1	0	0
σ_{III}'	0	$\cos\beta$	$-\sin\beta$	ε_{III}'	0	$\cos\alpha$	$-\sin\alpha$

Then, in matrix notation the stresses in the rotated principal stress axes system can be related to the material axes by,

$$\{\sigma_i\} = [T_\sigma]\ \{\bar{\sigma}_i'\} \tag{23}$$

where $[T_\sigma]$ is the transformation matrix which can be written,

$$[T_\sigma] = \begin{bmatrix} 0 & \sin^2\beta & \cos^2\beta & 2\cos\beta\sin\beta & 0 & 0 \\ 1 & 0 & 0 & 0 & 0 & 0 \\ 0 & \cos^2\beta & \sin^2\beta & -2\cos\beta\sin\beta & 0 & 0 \\ 0 & 0 & 0 & 0 & -\sin\beta & -\cos\beta \\ 0 & \cos\beta\sin\beta & -\sin\beta\cos\beta & \cos^2\beta-\sin^2\beta & 0 & 0 \\ 0 & 0 & 0 & 0 & \cos\beta & \sin\beta \end{bmatrix} \tag{24}$$

The strains transform under the same rules but the transformation matrix will be different because of the factor of 2 in the vector strains. Also because the principal stresses and strains are not coincident, the direction cosines are now in terms of the angle α. The transformation matrix for strain can be written,

$$[T_\varepsilon] = \begin{bmatrix} 0 & \sin^2\alpha & \cos^2\alpha & \sin\alpha\cos\alpha & 0 & 0 \\ 1 & 0 & 0 & 0 & 0 & 0 \\ 0 & \cos^2\alpha & \sin^2\alpha & -\cos\alpha\sin\alpha & 0 & 0 \\ 0 & 0 & 0 & 0 & -\sin\alpha & \cos\alpha \\ 0 & 2\cos\alpha\sin\alpha & -2\sin\alpha\cos\alpha & \cos^2\alpha-\sin^2\alpha & 0 & 0 \\ 0 & 0 & 0 & 0 & \cos\alpha & \sin\alpha \end{bmatrix} \tag{25}$$

In matrix notation the transformation of strains can be written,

$$\{\varepsilon_i\} = [T_\varepsilon]\ \{\bar{\varepsilon}_i'\} \tag{26}$$

By relating the strain and stress vectors for the material axes system with the compliance matrix,

$$\{\varepsilon_i\} = [C_{ij}]\ \{\sigma_i\} \tag{27}$$

and substituting the transformed quantities,

$$[T_\varepsilon]\ \{\bar{\varepsilon}_i'\} = [C_{ij}]\ [T_\sigma]\ \{\bar{\sigma}_i'\} \tag{28}$$

the elastic compliance matrix can be solved with respect to the principal material axes.

The compliance matrix can be written in terms of Hooke's law using the material properties of Young's modulus, E, and Poisson's ratio, ν. For the special case of cross anisotropy where the direction of consolidation is the axis of symmetry, the material properties in planes normal to the axis of symmetry will be isotropic. It can be shown that the compliance matrix reduces to the following,

$$[C] = \begin{bmatrix} 1/E & -\nu/E & -\nu'/E' & 0 & 0 & 0 \\ -\nu/E & 1/E & -\nu'/E' & 0 & 0 & 0 \\ -\nu'/E' & -\nu'/E' & 1/E' & 0 & 0 & 0 \\ 0 & 0 & 0 & \frac{1}{G'} & 0 & 0 \\ 0 & 0 & 0 & 0 & \frac{1}{G'} & 0 \\ 0 & 0 & 0 & 0 & 0 & \frac{2(1+\nu)}{E} \end{bmatrix} \tag{29}$$

where ν and E refer to the properties in the plane of transverse isotropy and ν', G' and E' refer to the properties in the plane normal to the plane of isotropy. A cross anisotropic material has 5 independent elastic constants.

The data reduction technique described, demonstrates that by applying stresses to the hollow cylinder specimen in a controlled loading the magnitudes and directions of the principal stresses and strains can be calculated. The calculated principal stresses and strains can then be transformed to the principal material axes system and the compliance matrix relating stresses and strains can be determined.

Assessment of Capabilities

In principle, independent control of the magnitudes and direction of the principal stresses can be achieved by subjecting a hollow cylinder specimen to combinations of axial, torsional, and spherical stresses, but only at the expense of stress and strain nonuniformities across the wall. The nonuniformities can be reduced by judicious selection of the sample geometry, but there still remain areas in stress space where the hollow cylinder apparatus should be used with caution because of the higher level of nonuniformities which may develop. There is more credence to tests where the internal and external cell pressures are kept equal, however, this is at the expense of the independent control of the magnitude and direction of the intermediate principal stress, which is then always radial and equal to the cell pressure.

In addition to the usual end effects and associated stress nonuniformity discussed in the preceding paragraphs, stress nonuniformity caused by the cross anisotropy of the specimen coupled with end constraints can develop. This non-uniformity is caused by the tendency for a specimen, that is tested with the principal stress directions oriented at an angle β with respect to the material axes, to develop shear and normal stresses on the principal material planes. The shear stresses and corresponding shear strains result in a skewed deformation response of the specimen. The rigid end platten constraints on

the specimen inhibit this shear response and result in a net lateral shear stress being applied to the ends of the specimen. To preserve equilibrium, the normal stress distribution on the specimen ends must become skewed. This would result in bending normal to the axis of the specimen as the top end of the specimen is offset from the bottom end. The nonuniformity in the stress distributions can be quite pronounced and large enough to lead to serious errors in interpreting test results. In particular, a localized failure may be precipitated and the stress state at which failure occurs may be underestimated.

Stresses and strains must be indirectly calculated as average values from expressions derived from assumptions that the cylindrical specimen is thin walled and behaves linear-elastically. Simultaneous variation of four stresses in the most general case to follow complex predefined stress paths is clearly a formidable undertaking, not to mention a major computational effort during the test.

A principal difficulty is the procurement of relatively large undisturbed specimens, whose principal material axes are coincident with the axes of the apparatus. Also, possible boundary disturbance effects resulting from the need to trim relatively thin walled hollow cylinders must be considered.

The above limitations are minor in view of the benefits obtained with the use of the hollow cylinder apparatus for measuring anisotropy of strength. Stress induced specimen

anisotropy, which exists solely from application of shear due to initial deposition of the clay particles and subsequent K_o-consolidation, can be investigated by performing tests in which strength and deformation characteristics independent of the intermediate principal stress are observed for different but constant values of the orientation of the major principal stress. Investigation of the effects of the intermediate principal stress is made more difficult by the restriction that the cell pressures be equal. Two tests with a constant b value and hence a constant inclination of the principal stresses on the axis of symmetry would have to be conducted. One test at a constant intermediate principal stress and the other with a variable one would be necessary to study the effects of the intermediate principal stress.

While this report is not intended to cover cyclic testing, it is noteworthy that the hollow cylinder apparatus has the capability of rotating the principal stresses in a continuous fashion, which is practical for the analysis of the response of soils beneath offshore structures under wave loading. Rotating the principal stresses continuously results in strains whose rotations are due to both anisotropy and the changes in the direction of the stress, with no possibility of separating them. It is only by maintaining the direction of the stresses constant and measuring the strains, or vice versa,

that one can employ the data reduction procedure discussed herein for the investigation of anisotropy.

CHAPTER III

TRULY TRIAXIAL APPARATUSES

Stress Application in the Truly Triaxial Apparatus

The truly triaxial apparatus permits the application of three independent, normal principal stresses to a prismatic specimen of cubic or parallelepiped shape. Three approaches have been used for the application of loads: rigid flat plattens for displacement controlled boundaries, flexible membranes for stress controlled boundaries, or a combination of both. Table 2 contains an assessment of the advantages and disadvantages of the three types of boundary conditions (32). None of the approaches is the most suitable for testing all types of soils over a wide range of stress or strain paths.

For the investigation of anisotropic soils, stresses applied through flexible membranes assure that a principal stress state is maintained on all faces while permitting unrestrained normal and shear distortion. It is this variation of the apparatus that is illustrated in Figure 16.

Stress and Strain Distribution in the Triaxial Specimen

The flexibility of the membrane in following the changing shape of the specimen while continuing to apply a uniform normal stress generated by pneumatic or hydraulic pressure avoids many

Table 2

Comparison of Boundary Conditions (32)

Strain Controlled: All Rigid Boundaries	Stress Controlled: All Flexible Boundaries	Mixed (Rigid and Flexible) Boundary Conditions
Advantages		
(a) Strains can be measured accurately	(a) Normal, principal stresses assured on the loading faces	(a) Boundary interference is usually avoided by assigning the rigid boundary as the compressive deviator direction and stress-controlled flexible boundary as extension deviator direction
(b) Uniform strains are possible	(b) Uniform stress distribution over all faces is possible	(b) Pore water pressure and other facilities are easily accommodated
(c) Large uniaxial strains can be achieved.	(c) Large strain can be achieved in three dimensions without significant boundary interference	(c) Stress or strain paths can be easily followed if a predetermined selection of specimen orientation with respect to apparatus axes is allowed
(d) Complicated and predetermined strain paths can be readily modeled	(d) Complicated and predetermined stress paths can be readily followed	(d) Plane strain tests can be modeled
(3) Pressure cells and pore water pressure instrumentation can easily be accommodated in the loading platens.	(e) Shear distortions are possible and measurable	

Table 2 (continued)

Strain Controlled: All Rigid Boundaries	Stress Controlled: All Flexible Boundaries	Mixed (Rigid and Flexible) Boundary Conditions
	Disadvantages	
(a) The uniformity of stresses induced is difficult to verify	(a) Interference at boundaries can occur if proper precautions are not taken	(a) Complicated predetermined stress or strain paths are difficult or impossible to follow
(b) Apparatus will not accommodate or allow shear distortions	(b) The uniformity of large strains can be difficult to maintain if proper lubrication is not performed	(b) Uniformity of stress and strain fields in directions normal to rigid and flexible boundaries difficult to ascertain
(c) Loading platen interference occurs at large multiaxial strain states	(c) Difficult to follow predetermined strain paths	(c) Heterogeneous stress and strain fields occur near boundaries
(d) Difficult to follow predetermined stress paths	(d) Plane strain experiments can only be achieved through stepwise corrections of stress state normal to plane	(d) Apparatus is usually large and unwieldy
(e) Apparatus is usually large and unwieldy	(e) Pore water pressure facilities are not easily accommodated	(e) Operation is usually extremely complicated
(f) Operation is usually complicated		(f) Apparatus will not allow shear distortions

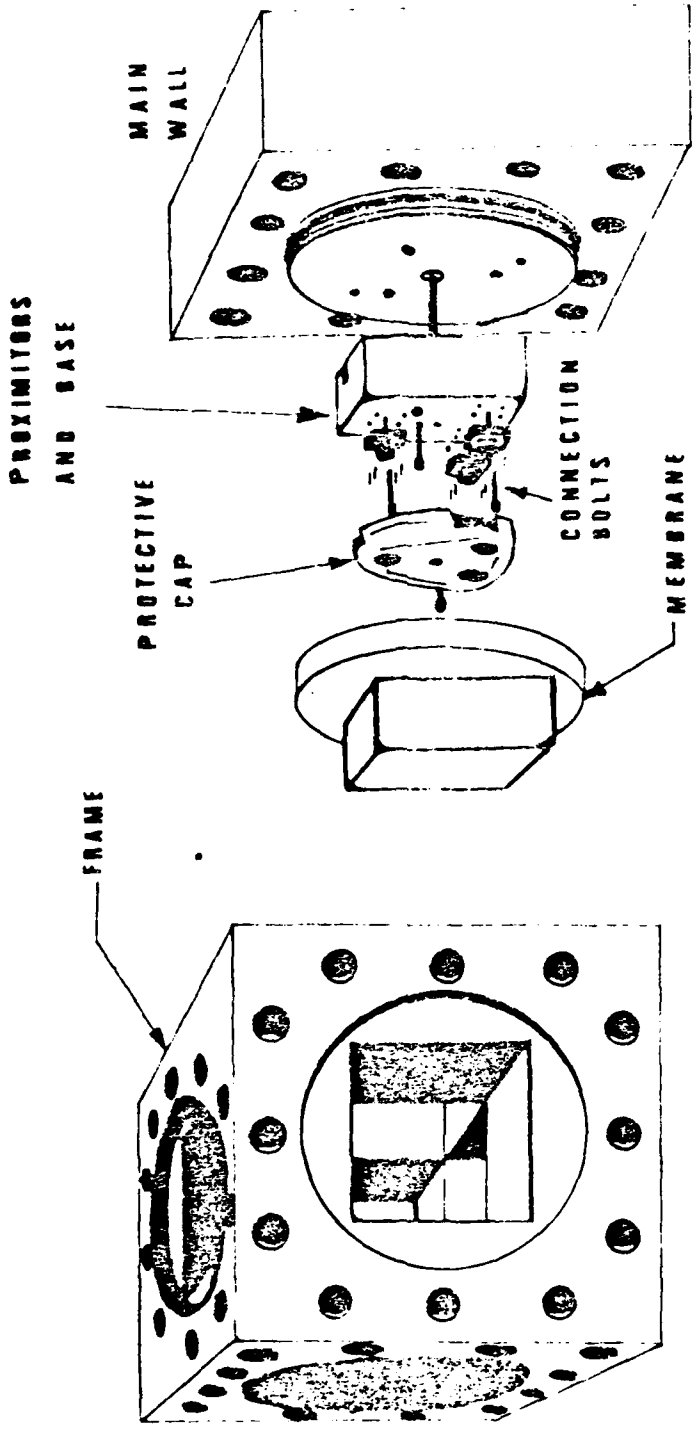

Figure 16. Exploded View of the Truly Triaxial Apparatus (31)

of the undesirable boundary effects associated with rigid loading plattens. Frictional restraint between the membranes and the specimen, which would result in shear stresses on the face of the specimen, is effectively minimized by lubrication or the use of teflon sheet interfaces. Practically unrestrained deformation assures uniformity of stresses and strains within the specimen. Shear stresses can be expected to be less than 5% of the applied normal stress (31).

The applied loads and deformations can be measured directly and accurately. The deformations of the specimen are recorded by deformation detecting transducers (proximity transducers) mounted three on each face in order that both normal displacements and shear deformations can be monitored. The normal displacements are calculated as the average of the three transducer readings at each face. The plane of the skewed specimen face is defined by the positions of the three transducers monitoring that face. Therefore, two sets of transducers on adjacent faces can detect the shear distortion of the right angle between those two faces. The total of eighteen readings define the complete strain state of the specimen, providing three normal and three shear strains.

The well controlled and known boundary conditions of the fluid cushion truly triaxial apparatus coupled with the facilities for determining the six components of strain provide sufficient information for the determination of the material

compliance matric, $[C_{ij}]$, relating stresses to strains. Since the directions of the principal stresses are not rotatable, the determination of the compliance matrix for a cross anisotropic material requires testing of specimens trimmed at oblique orientations to the principal material axes. The principal normal stresses applied to the nonprincipal material planes can be resolved into components of shear stresses and normal stresses on the principal material planes. Likewise, the measured normal and shear strains can be transformed to refer to the material axes system. The data reduction procedure would be the same as that described in Chapter II for the hollow cylinder specimen provided the direction of one of the material axes of the oblique specimen does not change. Usually, the direction of one of the horizontal axes in the plane of transverse isotropy will remain fixed.

The use of an obliquely oriented specimen to simulate the rotation of the principal stresses results in significant limitations in the method of reconsolidation to that stress state existing in situ. A typical clay specimen which has the property of cross anisotropy can be K_o-reconsolidated in the truly triaxial apparatus when the axes of the applied principal stresses and the in situ principal stresses are coincident. When the axes do not coincide, as would be the case of an obliquely oriented specimen, anisotropic consolidation causes shear stresses on the principal material planes. These shear stresses will

result in sample disturbance in the form of changes in the structure and the fabric of the specimen caused by shear distortions. The potential of disturbing the specimen increases as the value of K_o deviates from unity, as the specimen's material axes approaches 45° with respect to the principal stress axes of the apparatus, and with increasing sensitivity of the sample.

To minimize the disturbance of an obliquely oriented specimen, the researcher can reconsolidate the sample under isotropic stress conditions. This approach may minimize the disturbance of the sample, however, the shear strength and deformation characteristics may not be at all similar to those of the in situ soil. Donaghe and Townsend (6) in their study of the effects of anisotropic versus isotropic reconsolidation of initially K_o-consolidated clay concluded that for a given major principal consolidation stress, anisotropic consolidation produces a higher water content and hence a lower shear strength at $(\sigma_1-\sigma_3)_{max}$ than does isotropic consolidation of the same specimen. For the two clays tested, the maximum reductions in strength amounted to 9 and 15%. The results also indicate that if failure is instead defined at the maximum principal stress ratio, $(\sigma_1'/\sigma_3')_{max}$, the method of consolidation had no effect on the effective angle of internal friction, θ', for normally consolidated clays. This suggests that the possible differences in strength due to changes in structure resulting from the

method of consolidation are obliterated by the additional shearing action required to develop $(\sigma_1'/\sigma_3')_{max}$ values. The study also found that the stress-strain characteristics were significantly affected by the value of K_o. The axial strain values at $(\sigma_1-\sigma_3)_{max}$ generally decreased with decreasing values of K_o. The greatest reductions were up to 98% and they occured in the normally consolidated range. Hence, analyses requiring strength and stress-strain constitutive relations, such as finite elements methods, will be greatly affected by the consolidation ratio while, on the other hand, limiting equilibrium analyses at $(\sigma_1'/\sigma_3')_{max}$ will be unaffected by the consolidation ratio.

The maximum strain and shear distortion are limited by the design of the apparatus. The specimen may deform to the point that it interfers with the corners and edges of the frame of the cell or the membranes' capability to follow the deforming specimen is exceeded. In either case the resulting stress nonuniformities would invalidate the test.

Assessment of Capabilities

The truly triaxial apparatus with flexible membrane boundaries is capable of applying uniform and independently controlled three-dimensional stress states to a cubical specimen. Except for 90° jump rotations, the apparatus is not able to change the direction of the principal stress axes. The alternative is to test specimens trimmed at various angles with

respect to the principal material axes. However, anisotropic consolidation of obliquely oriented specimens results in fabric disturbance. Alternative isotropic consolidation may or may not be a realistic starting point for a test.

Because of the well controlled and known boundary conditions, the loads and deformations, including shear distortion, can be measured accurately. Experimental procedure and theory for the determination of the constitutive relations have been applied to anisotropic materials (12).

Unlike the hollow cylinder apparatus, the triaxial device is not strictly limited to size dictated by stress uniformity requirements. It has been demonstrated that larger cubical specimens, seven inches compared to four inches on a side, result in better average stress uniformity across specimens of sand (19). However, for clays this would increase the consolidation time for a consolidated undrained test to unreasonable duration.

The apparatus under manual or computer control of the loads, is able to follow a predetermined stress path with a high degree of accuracy. In this regard, the only limitations are due to the maximum strains and shear distortions, which are on the order of 9% for most apparatuses (2).

CHAPTER IV

MECHANICAL BEHAVIOR OF K_o-CONSOLIDATED CLAYS

A literature review of available published work revealed that the mechnaical behavior of saturated clay soils has, for the most part, been investigated within a framework valid only for isotropic materials.

The earliest studies of the effects of K_o-consolidation and its resulting anisotropy were conducted using standard triaxial cells and specimens cut at various inclinations to the direction of consolidation. Using this procedure, Duncan and Seed (7, 8) found that the undrained shear strength and excess pore water pressure varied with the specimen's inclination, but the values of the shear strength parameters, c' and θ', in terms of effective stress were constant and independent of inclination. Studies made by other investigators using different clays had similar findings but with different forms of variation of the undrained shear strength. The conclusions drawn from these tests have been seriously questioned because of the bendings and shears generated at the ends of the specimens by the presence of anisotropy (26).

The truly triaxial apparatus with flexible membranes offers the opportunity to study general mechanical behavior

but limitations in K_o-consolidation and difficulty in incorporating devices for pore pressure measurements are probably the primary reasons that the published results of undrained anisotropic behavior of clays are not readily available. Appendix A summarizes the results of the author's laboratory work demonstrating the use of one of the truly triaxial apparatuses used at the University of Colorado, Boulder for study of anisotropic behavior.

One of the most published studies of the mechanical behavior of clays is that by Saada and his co-workers using the hollow cylinder apparatus (23, 24, 25, 27). Selected results from these studies will be the focus of this chapter.

Materials and Testing Procedures

The tests were conducted in a hollow cylinder apparatus controlled by a pneumatic, analog computer. The specimens were subjected in an undrained condition to combinations of axial and torsional stresses at constant ratio. This was necessary to keep the inclination, β, of the major principal stress with respect to the direction of consolidation constant during a given test. The internal and external cell pressures were kept equal for the sake of uniformity of radial stresses in the wall of the specimen. This restriction does not allow for the independent control of the intermediate principal stress and confines the possible stress states to those shown in Figure 12.

Unfortunately, this restriction also prevents one from observing specific trends in the behavior, although cautious conclusions can be drawn.

For the first series of tests, specimens of a Florida clay called Edgar Plastic Kaolin were prepared by initial K_o-consolidation of clay slurry in a large consolidometer and final K_o-consolidation in the testing apparatus. At the end of the consolidation process the specimens were left to rebound and reach equilibrium at the desired cell pressure. Rebound to a hydrostatic state of stress was made necessary by the fact that subsequent undrained testing had to proceed with both the axial and torsional stresses increasing simultaneously and at a constant ratio. Thus all samples were in a lightly overconsolidated state prior to testing.

In the second selected series, tests were conducted on specimens of the same Florida clay obtained by consolidation of clay slurries in a large consolidometer. Three different degrees of anisotropy were achieved by giving the final consolidation pressure three different values. At the end of the consolidation process, the specimens were removed and placed in the hollow cylinder apparatus where consolidation was continued under a hydrostatic state of stress. All the specimens were normally consolidated in this fashion prior to testing.

The above two series of tests were chosen because they were representative of anisotropic behavior and also because the published results were most complete.

Each test series consisted of thirteen different total stress paths and seven inclinations of the principal stresses on the axis of symmetry, which was parallel to the vertical axis of the specimen. The total stress paths followed are shown on a p-q diagram in Figure 17 and on a τ_{oct}-σ_{oct} diagram shown in Figure 18. The octahedral shear stress and normal stress, τ_{oct} and σ_{oct} respectively, take into account the intermediate principal stress. The letters and numbers on each line identify the type of test from Table 3 and the inclination of the major principal stress.

Results and Analysis

Results of the Florida clay experimental investigation are listed in Tables 4 and 5 for the first and second series respectively. Complete test results are published in references (24) and (27).

Reading down each column in Tables 4 and 5, the magnitudes of the undrained strength are seen to change substantially with the direction of the principal stress, indicating the dependence of the undrained strength on the inclination of the principal stress. By reading across Table 5 for the normally consolidated tests all initiated at the same confining pressure,

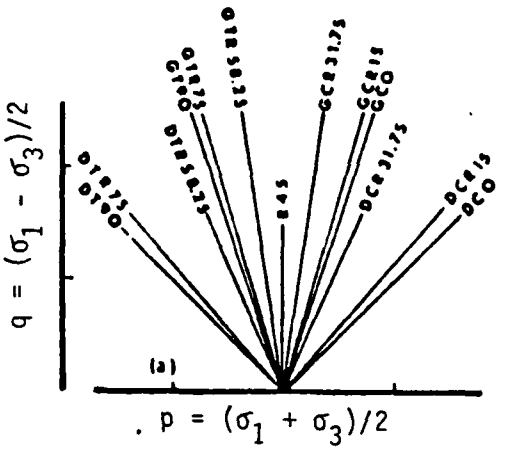

Figure 17. Total Stress Paths in P—q Space (24)

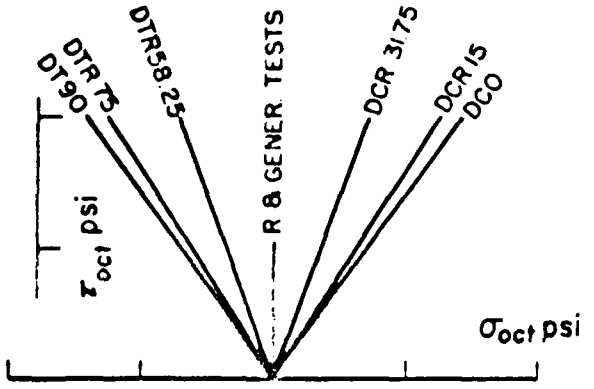

$$\tau_{oct} = \frac{1}{3}\left[(\sigma_1-\sigma_3)^2+(\sigma_2-\sigma_3)^2+(\sigma_3-\sigma_1)^2\right]^{1/2} \quad (29)$$

$$\sigma_{oct} = \frac{1}{3}(\sigma_1+\sigma_2+\sigma_3) \quad (30)$$

Figure 18. Total Stress Paths in $\tau_{oct}-\sigma_{oct}$ Space (27)

Table 3. Designation of Tests Conducted (27)

	Type of Specimen	β^{o}		Loading System	Designation
Direct Tests	Horizontal	90	Cell Pressure	axial stress increase	D.C. H
	Vertical	0	is constant.	axial stress increase	D.C. 0
	Vertical	15	Mean stress	axial stress increase+torque	D.C.R.15
	Vertical	31.7	is variable	axial stress increase+torque	D.C.R.31.7
	Vertical	58.2		axial stress decrease+torque	D.T.R.58.2
	Vertical	75		axial stress decrease+torque	D.T.R.75
	Vertical	90		axial stress decrease	D.T. 90
Generalized Tests	Vertical	0	Cell Pressure	axial stress increase	G.C. 0
	Vertical	15	is variable.	axial stress increase+torque	G.C.R.15
	Vertical	31.7	Mean stress	axial stress increase+torque	G.C.R.31.7
	Vertical	58.2	is constant.	axial stress decrease+torque	G.T.R.58.2
	Vertical	75		axial stress decrease+torque	G.T.R.75
	Vertical	90		axial stress decrease	G.T. 90
Torsion	Vertical	45		torque	R. 45

Table 4. Results of First Test Series (24)

test type	β in ^{o}	Florida-1			Florida-2			Florida-3		
		q_f (psi)	τ_{oct} (psi)	ϕ in ^{o}	q_f (psi)	τ_{oct} (psi)	ϕ in ^{o}	q_f (psi)	τ_{oct} (psi)	ϕ in ^{o}
DC	0	39.8	37.5	26.7	39.1	36.9	30.9	28.6	27.0	32.1
GC	0	41.0	38.6	26.8	34.9	32.9	30.1	28.4	26.8	32.4
DCR	15	49.9	45.5	31.7	41.3	37.7	34.0	30.2	27.6	36.6
GCR	15	51.6	47.1	33.3	38.5	35.1	33.7	22.9	20.9	32.2
DCR	31.75	49.1	41.4	37.0	36.8	31.0	39.1	30.6	25.8	46.4
GCR	31.75	50.5	42.6	38.9	40.6	34.2	40.8	24.6	20.7	40.6
R	45	46.2	37.7	45.5	37.2	30.4	45.2	26.4	21.6	51.8
DTR	58.25	40.5	34.1	40.6	30.2	25.5	42.5	21.6	18.2	45.3
GTR	58.25	39.4	33.2	39.6	32.9	27.7	44.8	18.9	15.9	41.0
DTR	75	36.3	33.1	40.7	28.6	26.1	45.8	20.1	18.3	51.4
GTR	75	37.3	34.1	41.3	31.2	28.5	44.9	20.5	18.7	47.3
DT	90	34.2	32.2	39.8	27.0	25.5	43.5	19.9	18.7	54.9
GT	90	32.4	30.5	36.5	29.3	27.6	45.4	21.1	19.9	53.1
Consolidation cell pressure			80			60			40	
K_o			0.47			0.46			0.48	

Table 5. Results of Second Test Series (27)

Type of test	β in ^{o}	Florida-4				Florida-5				Florida-6			
		q_f (psi)	τ_{oct} (psi)	ϕ (^{o})	$3a_f$	q_f (psi)	τ_{oct} (psi)	ϕ (^{o})	$3a_f$	q_f (psi)	τ_{oct} (psi)	ϕ (^{o})	$3a_f$
DC	0	51.5	24.2	31	.79	57.0	26.9	31	.56	58.9	27.8	31	.46
GC	0	50.5	23.8	31	.86	57.3	27.0	32	.59	61.1	28.8	32	.45
DCR	15	55.4	25.2	34	.73	58.5	26.7	35	.66	60.8	27.7	33	.47
GCR	15	52.0	23.7	34	.88	57.5	26.2	35	.68	62.4	28.5	35	.50
DCR	31.7	49.6	20.9	36	1.04	61.5	25.9	40	.67	62.9	26.5	40	.59
GCR	31.7	50.1	21.1	37	1.04	59.9	25.3	41	.75	60.8	25.6	41	.71
DTR	58.2	50.3	21.2	39	.78	51.5	21.7	41	.77	55.9	23.6	43	.64
GTR	58.2	48.9	20.6	37	.76	52.7	22.2	42	.74	56.4	23.7	46	.69
DTR	75	48.3	22.0	47	.90	49.4	22.5	43	.73	53.4	24.3	49	.69
GTR	75	46.5	21.2	45	.96	49.6	22.7	44	.74	55.1	25.1	44	.49
DT	90	45.3	21.3	43	.89	48.7	22.9	43	.72	50.5	23.8	46	.70
GT	90	43.5	20.5	40	.93	50.5	23.8	47	.71	50.0	23.6	44	.67
R	45	50.4	20.6	40	1.00	56.0	22.9	42	.79	59.0	24.1	43	.70

the undrained strength is also seen to be dependent on the degree of anisotropy.

Figures 19, 20, and 21 graphically show the different effective stress paths for the tests in the first series. The number on each curve corresponds to the order in which the test appears in Table 3. In each group, every inclination of the principal stress corresponds to a different effective stress path and to a different octahedral shear stress at failure. The tests in which the specimens are axially compressed fall on one side of the effective path for pure torsion, and those in which the specimens are axially elongated fall on the other side.

All the axial stress-strain curves of the specimens in the first series indicate that for the same levels of stress, as well as at the failure stress, the axial strains are much larger when extensions are involved. Figure 22 shows the results of a compression and an extension test conducted on Florida-2 clay. In the compression test, one where the major principal stress and the direction of consolidation are parallel, the specimen is much stiffer compared to the extension test where the major principal stress is normal to the direction of consolidation. Such results are typical and show the extent of the difference in response of cross anisotropic specimens, depending on whether they are compressed or elongated along their axis of symmetry.

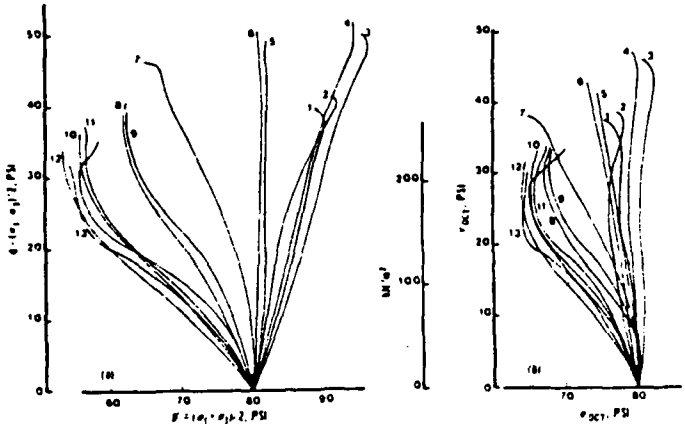

Figure 19. Effective Stress Paths for Florida-1 Clay (24)

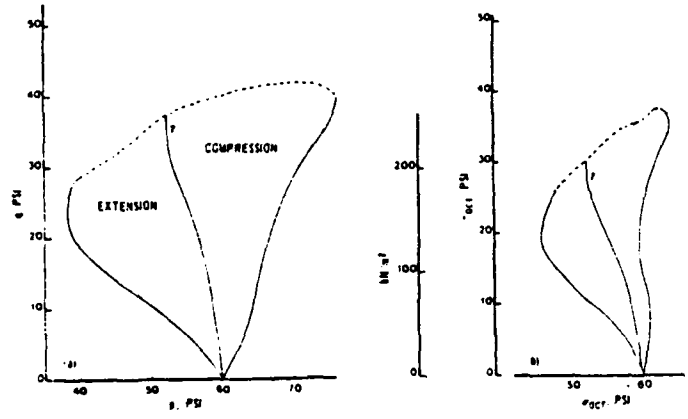

Figure 20. Effective Stress Paths for Florida-2 Clay (24)

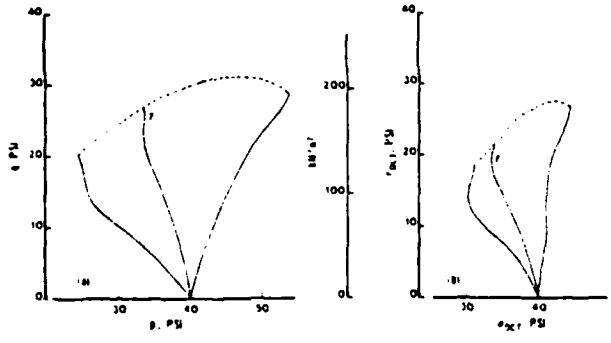

Figure 21. Effective Stress Paths for Florida-3 Clay (24)

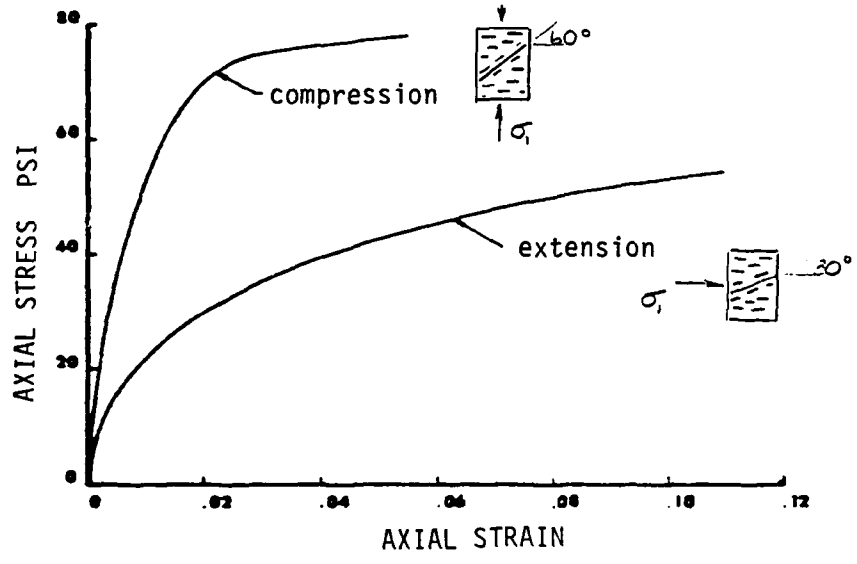

Figure 22. Axial Stress-Strain Curve (25)

The friction angle in terms of effective stress, $\emptyset'$, varies with the stress path, and with the degree of anisotropy by as much as 50%. The results of both tables show that the values of $\emptyset'$ obtained from a CDO test, that is a direct test in which the specimen's axis of symmetry and the major principal stress direction coincide and which duplicates a standard triaxial compression test, are consistently the smallest. Hence, soil bearing capacity and stability analyses dependent on the soil parameter $\emptyset'$ determined by conventional triaxial compression test results would be conservative for cross anisotropic clays. From the design safety point of view this is comforting but it does indicate the considerable amount of error that may be built into an analysis using isotropic strength parameters. It is noteworthy that the calculated variations in the friction angle are a direct consequence of the Mohr-Coulomb failure criterion used by Saada to define the parameter, and may be only partially due to the mechanisms involved in the deformations of anisotropic soils. The fact that the analytical expression for $\emptyset'$ is independent of the intermediate principal stress, makes it suspect as a true indication of the variation of the frictional component of shear strength.

From the second series of results, Table 5, it is apparent that Henkel's pore pressure coefficient at failure, a_f, depends on the stress path as well as on the direction of the principal stress. The value of a_f decreases with the

increasing degree of anisotropy. The pore pressure parameter is also always higher for tests where the principal stress is horizontal rather than for tests where it is vertical. For undrained tests, the excess pore water pressure is a measure of the tendency of the material to change volume. Thus, it can be said that for horizontal inclinations of the major principal stress, there is a greater tendency for volume change.

From the results presented one can conclude that for a K_o-consolidated, consequently a cross anisotropic clay, undrained strength and effective stress path depend not only on the initial conditions existing before shear, but also on the way shear is applied. The degree of anisotropy induced by one-dimensional consolidation can not be ignored.

A fuller understanding of the effects of anisotropy and the reorientation of the principal stress directions on the undrained strengths of clay is achieved by a review of the fundamental aspects of the physiochemical behavior of clay leading up to the mechanisms for development of shear strength.

Clay Structure Development

Material structure is that property of the soil which provides the integrity of the system and which is responsible for response to externally applied sets of forces. Structure, therefore, includes the combined effects of particle arrangements, mineral composition, and interparticle forces. The geometrical

aspects of particle arrangements at a microscopic level are usually termed fabric. Researchers have observed that individual clay particles in suspension tend to form various particle associations, fabric units, which can be attributed to the net result of the interparticle forces of attraction and repulsion. In cases where the net curve of interaction exhibits a high repulsive energy, particles in suspension will be stable and the fabric is best described as dispersed and deflocculated or random. In cases where the repulsive energy barrier does not exist, particles are drawn into close proximity and flocculation results. Flocculated fabric units are characterized by edge-to-surface and edge-to-edge associations of several particles without any specific orientation. Particle associations in young deposits at high void ratios and in underconsolidated deposits assume a variety of forms, but most of them are related to the random or flocculated associations shown in Figure 23.

Using microscopy and X-ray diffraction methods, researchers have been able to observe changes in the inherent fabric of a soil mass as it undergoes one-dimensional consolidation. The observed sequential pattern of stress-induced fabric change shown in Figure 24 is as follows (36):

(1) rearrangement and reorientation of fabric units without any significant distortion of the units;

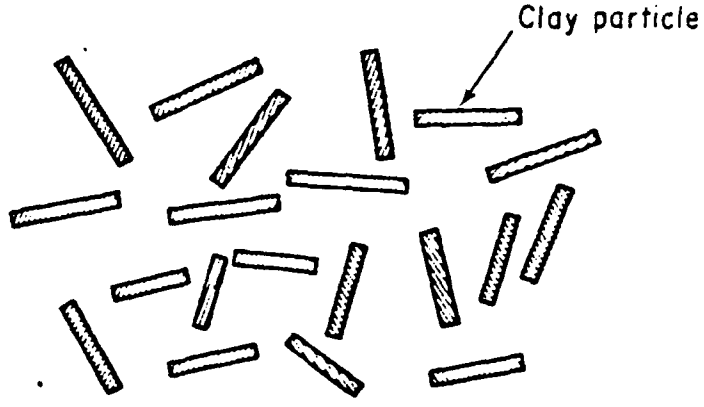

Random

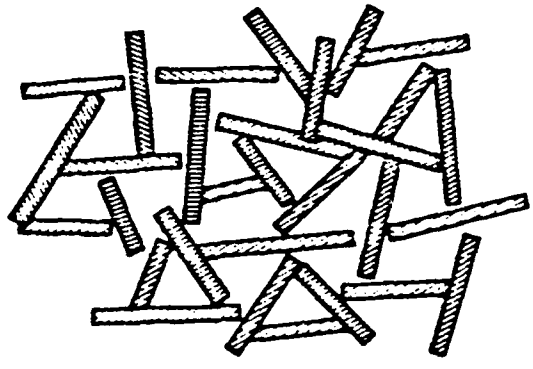

Flocculated

Figure 23. Idealized Clay Structures (36)

(1) Initial orientation of fabric units

(2) Reorientation of fabric units only - Some preferred orientation of particles

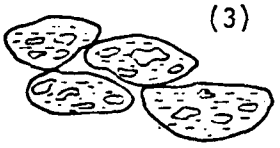

(3) Orientation of fabric units and particles in the fabric units

Figure 24. Effects of K_o-consolidation on Fabric (36)

(2) increased loading causes a greater degree of orientation of the fabric units. At this stage, some particle arrangement within the fabric units can occur;

(3) further loading causes more orientation of the fabric units and the particles within the fabric units.

The increase in compressive stress necessary to achieve higher degrees of fabric change is dependent on the structural metastability of the fabric units and the strength of the inter-particle bonds. For example, stresses as low as 10 kN/m^2 (0.1 $tons/ft^2$) may be sufficient to develop intense preferred orientation of a flocculated Kaolinite, however, considerably higher stresses may be needed in the case of clays with strong inorganic or organic bonds between particles (17). It is also logical that the load due to increasing overburden with depth would result in increasing degrees of anisotropy with depth.

Fabric Changes During Shear

Many aspects of the shear strength properties of clay soils are related to the fabric changes associated with the well-defined narrow shear zone that accompanies failure.

The development of shear induced fabric changes has been documented by Morgenstern and Tchalenko (18) in natural clays, and by Barden (1) in laboratory specimens. Some conclusions about fabric orientation in the shear zone have been reached.

Detailed examination of the fabric before peak shear strength was reached revealed no trace of discontinuities, but did show the development of a dominant shear zone. This zone had the structure X Y Z Y X illustrated in Figure 25. X is the original stress-induced fabric that was the result of K_o-consolidation. Y and Y are continuous shear planes, called principal displacement shear planes, that are located close to or at the boundaries of the shear zone. Principal displacement shear planes typically range between 10 and 100 μm in thickness, and they are characterized by particles which rotate and become highly oriented parallel to the direction of movement. Z is a zone of discontinuous shear planes called Riedel shear bands, that are inclined with respect to the displacement shear planes. Their development depends on clay composition and the magnitude of displacement (18).

During yield after peak strength is reached, near perfect preferred orientation develops, but local deviations prevent failure at residual strength at the outset. Virtually perfect parallel alignment of particles is needed before the strength reduces to a residual value. The dominant mechanism of deformation is then a face-to-face sliding mechanism called basal plane slip.

Skempton (30) recognized five successive stages within the shear zone of stiff overconsolidated clays subjected to simple shear. The first stage, before peak strength is reached,

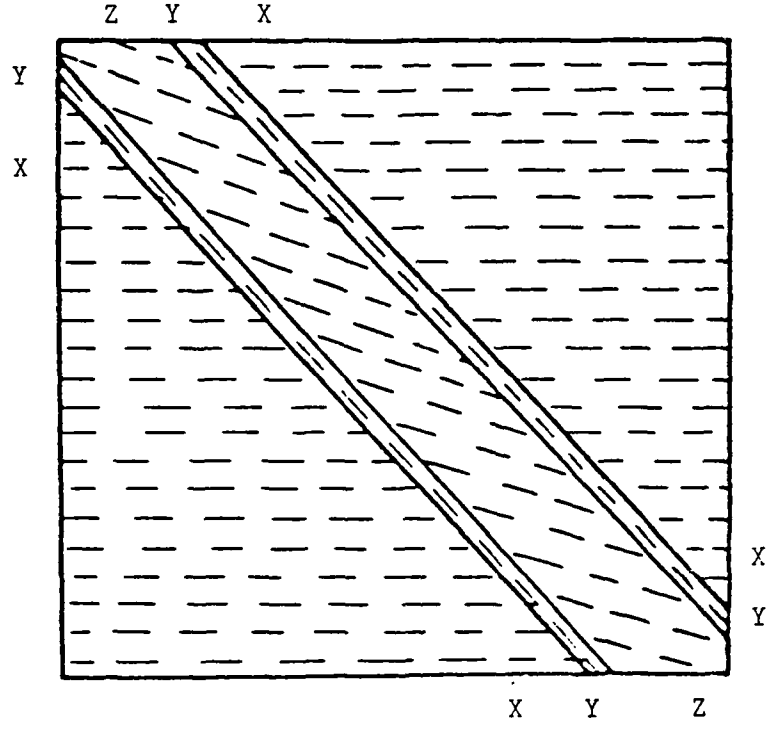

Figure 25. Structure of Failure Zone (1)

is one of continuous nonhomogeneous strain. In the second stage, which occurs at or just before peak, Riedel shear bands are formed as shown in Figure 26. They lie en echelon at an inclination usually between 10° and 30° to the direction of general movement. With further displacement, a third stage is soon reached at which the slip along the Riedel shear bands is no longer kinematically possible, and the clay is compelled to develop new slip surfaces parallel or subparallel to the direction of movement. These are the displacement shear planes. With greater movement, the displacement shear planes extend and eventually, in the fourth stage, some of them link up to form a principal displacement shear or slip surface. The surface is undulating since the shear planes involved were not originally all in line. Once a principal slip surface has formed, subsequent movement in the fifth stage causes the surface to undergo appreciable flattening. Large displacement can then take place without a fundamental change in the pattern of shear.

The above discussion assumes a homogeneous clay and does not consider the influence of possible macrostructures of a clay. Macrostructures, such as fissures, joints, slickensides, bedding planes, etc., act as weakening agents and can influence behavior on both the laboratory and field scale.

With a basic understanding of the changes of the microstructure within the narrow shear zone at failure, the development of shear strength can be explained.

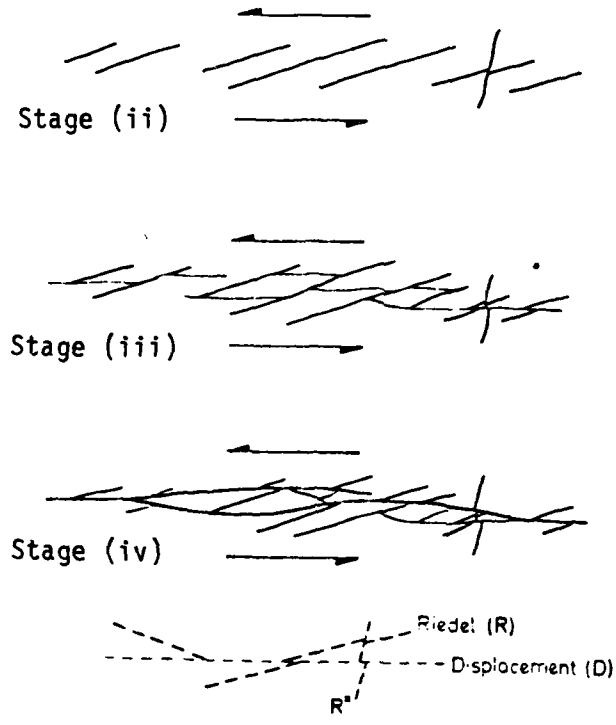

Figure 26. Stages of Shear Zone Development (30)

Mechanisms for the Development of Shear Strength

The development of shear resistance within the clay depends both on the arrangement of particles and particle groups, and on the forces holding them in place. If there is increased resistance to displacement and distortion of the fabric units under the action of applied shear, then greater strength may be found. It is possible on this basis to formulate a working hypothesis which would produce a mechanism for shear that appears to account for the effects of anisotropy and reorientation of the principal stress directions on the shear strength.

It has been suggested by Bjerrum (3) and others that shear strength is fundamentally composed of a true cohesion and friction that develop separately with strain. The cohesion component peaks at low strains while the friction component is mobilized gradually.

Cohesion may be defined as that component arising from the physiochemical forces of an interatomic, intermolecular, and interparticle nature (17). Respectively, these sources of cohesion are; van der Waals forces, electrostatic attractions between particle edges which are oppositely charged, and the chemical cementation characteristic of bonded clays. The principal difference between these bonds is that the cementation bonds are brittle and break down during shear, while the other two are at least partly redeveloped when new contact points

are established. They then can offer frictional resistance to displacement.

The frictional component of shear, is that caused by resistance to parallel arrangement and resistance to relative movement of sliding of one fabric unit over another. Frictional resistance can be considered as both a physiochemical, and a physical phenomenom highly dependent on the magnitude of the effective stress (36). Development of the displacement shear planes and Riedel shear bands requires the fabric units to become highly mobilized in the direction of movement. Adhesion and interlocking due to interparticle forces of attraction must be overcome if reorientation is to occur. If repulsive forces are dominant, then particle movement, which in many instances requires one fabric unit to move closer to another, will again be resisted. For unbonded clays at the same initial void ratio, highest shear strength will be measured where attraction is the dominant interparticle force. Evidence of a physical component of friction, that due to physical solid particle-to-particle contact, has come in the form of microphotographs of clay particle surfaces scratched during shear (16). For undrained tests, a further resistance to fabric unit arrangement may be provided through total pore pressure response, that is, pressures due to physical breakdown and reorientation of particles.

The above mechanisms of shear strength, coupled with the fabric changes in the shear zone discussed under a previous heading, lead to the following picture of what happens when a clay specimen is subjected to increasing shear strain. The very first part of the stress-strain curve is a measure of the cohesive resistance of the intact structure against a shear distortion, and the strain is essentially the result of an elastic deflection of the structure. As stresses and strains increase, the cementation bonds are broken and the frictional component is gradually mobilized. The maximum resistance that the structure can offer before peak strength, is highly dependent on the difficulty in reorientation of the fabric units in the shear zone. At the peak stress, the maximum strength of the structure is reached and principal displacement shear planes form as failures occur at contact points along the failure plane. The residual shear strength of the structure is then mobilized in the form of cohesive bonds that at least partially redevelop at newly established contact points and result in friction.

An example of strength derived from orientation in an anisotropic clay soil is illustrated in Figure 22, which shows the results of a direct compression test and extension test on Florida kaolin with a high degree of anisotropy. For the compression test, the developed shear zone was oriented at a 60° angle with respect to the bedding of the fabric units,

while for the extension test, the shear zone was 30° with respect to the bedding plane. The increase in strength for the compression test is due not only to developed interparticle forces under greater normal stress, but also to the difficulty in reorientation of the fabric units through a 60° angle. There is a sharp rise in shear strength due to friction to a peak point defined by rotation and reorientation of the fabric, following which the clay possesses strength in the form of basal plane slip along the shear plane. The reduced strength of the extension test reflects the smaller stress normal to the bedding plane and the minimal required reorientation of the fabric units. Because of the greater facility for slip along the shear plane, lower shear stress with correspondingly higher shear strain and greater pore water pressure results.

The initial statistical distribution of the orientation of the fabric units with respect to the orientation of the potential shear zone should logically effect the expected strength. Or said another way, higher degrees of anisotropy of fabric result in greater directional variation in undrained strength, a fact which the test results demonstrate.

In characterizing the strength anisotropy of K_o-consolidated clays, it is important to bear in mind that both the stress and strain path dependencies are reflected in the development of material resistance. The published results of the hollow cylinder apparatus tests on clays all seem to have

been performed using the same procedure, where the internal and external cell pressures are maintained equal. This restriction increases the confidence in the uniformity of stress across the specimen's wall, but does not allow the researcher to independently control the intermediate principal stress and principal stress direction. Without being able to separate these two influences in the limited amount of published test data, the prediction of trends in variation of strength is necessarily cautious.

CHAPTER V

SUMMARY AND CONCLUSIONS

The test results presented and the discussion of the mechanism for development of shear strength make it clear that the undrained strength of anisotropic clays is dependent on both the magnitude and the direction of the principal stresses with respect to the principal material axes. The proper test system for investigation of the effects of anisotropy must be capable of applying relatively uniform and well-defined three-dimensional states of stress and strain, and have the ability to control the direction of the major principal stress axes relative to the principal material axes. The hollow cylinder apparatus and the truly triaxial apparatus, both of which were reviewed and evaluated in this report, are valid laboratory testing devices which, with few limitations, fulfill the stated requirements.

The hollow cylinder apparatus applies different combinations of axial, spherical, and torsional stress to a relatively thin walled, cylindrical specimen. Interpretation of the stress and strain distributions requires the basic assumption that the specimen is a thin walled cylinder which behaves linear-elastically. On this basis, the shear strain

due to applied torque is assumed to vary linearly from the specimen's axis, and the stress distribution across the wall of the specimen also varies linearly. Although the hollow cylinder specimen is in fact not thin walled, these assumptions remain reasonably valid for small angles of twist due to applied torque, and for small differences between the inner and outer cell pressures. Thus, some stress states and rotations of the principal stress direction, which may or may not be critical to a specific test procedure, are not attainable because of the unacceptable nonuniformities which develop. Saada et al (23, 24, 25, 27), in their extensive investigation of the effects of anisotropy on the undrained behavior of clays, minimized the nonuniformities across the wall by using specimens whose longitudinal axis and axis of symmetry are coincident, and by restricting the cell pressures to be equal. This restriction on the cell pressures increases the confidence that the difference between the calculated and the real stress and strain averages are small. However, the stress axes rotation and the changes in the intermediate principal stress can not then be independently controlled.

The truly triaxial apparatus's greatest advantage is its ability to apply uniform and well-defined states of principal stress to a cubical specimen. The flexible stress controlled boundaries allow essentially unrestrained deformations which can be described by the results of direct measurement. The stress states and stress paths excluding continuous

principal axes rotation which can be investigated are in principle unlimited. In order to simulate principal stress axes rotation, tests must be performed on specimens trimmed at different orientations with respect to the material axes system. However, if duplication of the in situ stress state requires anisotropic K_o-reconsolidation of the oblique specimen, appreciable sample disturbance in the form of shear distortion will result. Especially in sensitive clays, sample disturbance tends to destroy the original structure of the clay fabric. This disturbance can for the most part be avoided by isotropic reconsolidation, which may or may not be a reasonable starting point for a particular clay depending on the ultimate purpose of the test results.

Both the hollow cylinder and the truly triaxial apparatuses offer significant advantages over the conventional triaxial apparatus in their ability to more accurately and realistically represent in situ conditions. The two former apparatuses are practical devices for the determination of the constitutive relations of soils.

This report is obviously a subjective review of the two apparatuses, both because of the inexperience of the author, and because of the limited published test results. More indepth insight into the capabilities and the limitations of the apparatuses could be gained if several researchers were to carry out the same set of tests with a wide variety of stress paths

on identical soil samples, also of a wide variety. From the observed differences in the apparatuses come the following general conclusions. Provided an undisturbed hollow cylinder specimen can be obtained, the hollow cylinder apparatus is most suited for the testing of relatively stiff specimens with high clay contents. Samples of this nature can be trimmed easily with minimal boundary disturbance, and are sufficiently stiff so as not to deform under self weight as they are placed in the testing apparatus. If the expected value of $(\sigma_1/\sigma_3)_{max}$ is less than 3, most stress states and rotations of the principal stress axes can be investigated within a range of acceptable nonuniformity. Still, this apparatus is best used where the primary purpose of the test program is to investigate the effect of principal stress rotation at the expense of independent control of the intermediate principal stress.

The truly triaxial apparatus can test a wider variety of soils. This is because of the ease with which samples can be trimmed, and because of the greater latitude for boundary disturbance. That is, the thickness of the disturbed zone due to sampling and trimming is small compared to the dimensions of the specimen. If the purpose of the test is to investigate the influence of the intermediate principal stress and 90° rotation of the principal stress axes, then the uniform and well-defined states of stress and strain make this device superior to the hollow cylinder apparatus. The truly triaxial

device is not as suitable for the investigation of the principal stress orientations, especially for those cases where anisotropic K_o-reconsolidation is required. Ultimately, the choice of the better apparatus depends on the in situ conditions to be investigated, the parameters to be measured, and the purpose of the test.

Bibliography

1. Barden, L., "Examples of Clay Structure and Its Influence on Engineering Behavior," Proceedings of the Roscoe Memorial Symposium, Cambridge University, March 1971, R. Parry, Ed., pp. 196-205.

2. Berends, B.E., "Development of a Multiaxial Testing Cell for Testing Cohesive Soils," M.S. Thesis, University of Colorado, 1977.

3. Bjerrum, L. and Kenney, T.C., "Effect of the Shear Behavior of Normally Consolidated Quick Clays," Proceedings of the Geotechnical Conference, Oslo, 1967, Vol. 2, pp. 19-27.

4. Broms, B.B. and Casbarian, A.O., "Effects of Rotation of the Principal Stress Axis and of the Intermediate Principal Stress on the Shear Strength," Proceedings of the 6th International Conference of Soil Mechanics and Foundation Engineering, Montreal, 1965, Vol. 2, pp. 179-183.

5. Calladine, C.R., "A Microstructural View of the Mechanical Properties of Saturated Clay," Geotechnique, Vol. 21, No. 4, 1971, pp. 391-405.

6. Donaghe, R.T., and Townsend, F.C., "Effects of Anisotropic Versus Isotropic Consolidation in Consolidated-Undrained Triaxial Compression Tests of Cohesive Soils," Geotechnical Testing Journal, GTJODJ, Vol. 1, No. 4, December 1978, pp. 173-189.

7. Duncan, J.M. and Seed, H.B. "Anisotropy and Stress Reorientation in Clay," Journal of the Soil Mechanics and Foundations Division, ASCE, Vol. 92, No. SM5, Proc. Paper 4903, September 1966, pp. 21-49.

8. Duncan, J.M. and Seed, H.B., "Strength Variation Along Failure Surfaces in Clay," Journal of the Soil Mechanics and Foundations Division, ASCE, Vol. 92, No. SM6, Proc. Paper 4971, November 1966, pp. 81-104.

9. Green, G.E., "Discussion Leader's Closing Comments: Session 3," Proceedings of the Roscoe Memorial Symposium, Cambridge University, March 1971, R. Parry, Ed., pp. 401-109.

10. Hight, D.W., Gens, A., and Symes, M.J., "The Development of a New Hollow Cylinder Apparatus for Investigating the Effects of Principal Stress Rotation in Soils," Imperial College, 1982.

11. Hvorslev, M.J., "Physical Components of the Shear Strength of Saturated Clays," Proceedings of the Research Conference on Shear Strength of Cohesive Clays, ASCE Miscellaneous Publication, Boulder, June 1960, pp. 169-265.

12. Ko, H.Y. and Sture, S., "Three-Dimensional Mechanical Characterization of Anisotropic Composites," Journal of Composite Materials, Vol. 8, April 1974, pp. 178-183.

13. Lade, P.V., "Torsion Shear Apparatus for Soil Testing," Laboratory Shear Strength of Soil, ASTM STP 740, R.N. Yong and F.C. Townsend, Eds., American Society for Testing and Materials, 1981, pp. 145-147.

14. Lade, P.V., "Discussion of Laboratory Shear Devices," Laboratory Shear Strength of Soil, ASTM STP 740, R.N. Yong and F.C. Townsend, Eds., American Society for Testing and Materials, 1981, pp. 643-652.

15. Lade, P.V. and Musante, H.M., "Three-Dimensional Behavior of Remolded Clay," Journal of the Geotechnical Engineering Division, ASCE, Vol. 104, No. GT2, Proc. Paper 13551, February 1978, pp. 193-209.

16. Matsui, T., Ito, T., Mitchell, J.K., and Abe, N., "Microscopic Study of Shear Mechanisms in Soil," Journal of the Soil Mechanics and Foundation Engineering Division, ASCE, Vol. 106, No. GT2, February 1980, pp. 137-152.

17. Mitchell, J.K., Fundamentals of Soil Behavior, John Wiley & Sons, Inc., New York, 1976.

18. Morgenstern, N.R. and Tchalenko, J.S., "Microstructural Observations on Shear Zones from Slips in Natural Clays," Proceedings of the Geotechnical Conference, Oslo, 1967, Vol. 1, pp. 147-152.

19. Mould, J.C., "Stress Induced Anisotropy in Sand and the Evaluation of a Multi-Surface Elasto-Plastic Material Model," Ph.D. Thesis, University of Colorado, 1983.

20. Pearce, J.A., "A New True Triaxial Apparatus," Proceedings of the Roscoe Memorial Symposium, Cambridge University, March 1971, R. Parry, Ed., pp. 330-339.

21. Popov, E.P., Introduction to Mechanics of Solids, Prentice Hall, Inc., Englewood Cliffs, New Jersey, 1976.

22. Poulos, S.J. "Discussion of Soil Testing Practices," Laboratory Shear Strength of Soil, ASTM STP 740, R.N. Yong and F.C. Townsend, Eds., American Society for Testing and Materials, 1981, pp. 659-677.

23. Saada, A.S. and Baah, A.K., "Deformation and Failure of a Cross Anisotropic Clay Under Combined Stresses," Proceedings of the Pan American Conference on Soil Mechanics and Foundation Engineering, Caracus, 1967, Vol. 1, pp. 67-88.

24. Saada, A.S. and Bianchini, G.F., "Strength of One-Dimensionally Consolidated Clays," Journal of the Geotechnical Engineering Division, ASCE, Vol. 101, No. GT11, Proc. Paper 11707, November 1975, pp. 1151-1164.

25. Saada, A.S. and Ou, C. "Strain-Stress Relations and Failure of Anisotropic Clays," Journal of the Soil Mechanics and Foundation Engineering Division, ASCE, Vol. 99, No. SM12, Proc. Paper 10225, December 1973, pp. 1091-1111.

26. Saada, A.S. and Townsend, F.C., "State of the Art: Laboratory Strength Testing of Soils," Laboratory Shear Strength of Soil, ASTM STP 740, R.N. Yong and F.C. Townsend, Eds., American Society for Testing and Materials, 1981, pp. 7-77.

27. Saada, A.S. and Zamani, K.K., "The Mechanical Behavior of Cross Anisotropic Clays," Proceedings of the 7th International Conference on Soil Mechanics and Foundation Engineering, Mexico, 1969, Vol. 1, pp. 351-359.

28. Scott, R.F., Principles of Soil Mechanics, Addison-Wesley Publishing Company, Inc., Reading, MA., 1963.

29. Shibata, T. and Karube, D. "Influence of the Variation of the Intermediate Principal Stress on the Mechanical Properties of Normally Consolidated Clays," Proceedings of the 6th International Conference of Soil Mechanics and Foundation Engineering, Montreal, 1965, Vol. 2, pp. 359-363.

30. Skempton, F.R.S. and Petley, D.J., "The Strength Along Structural Discontinuities," Proceedings of the Geotechnical Conference, Oslo, 1967, Vol. 2, pp. 29-46.

31. Sture, S. "An Improved Multiaxial Cubical Cell and its Application to the Testing of Anisotropic Materials," M.S. Thesis, University of Colorado, 1973.

32. Sture, S. and Desai, C.S. "Fluid Cushion Truly Triaxial or Multiaxial Testing Device," Geotechnical Testing Journal, Vol. 2, No. 1, March 1979, pp. 20-33.

33. Suklje, L. and Drnovsek, J., "Investigation of the Deformability of Soil Using Hollow Cylinders," Proceedings of the 6th International Conference of Soil Mechanics and Foundation Engineering, Montreal, 1965, Vol. 2, pp. 368-372.

34. Symes, M.J., Hight, D.W., and Gens, A., "Investigating Anisotropy and the Effects of Principal Stress Rotation and of the Intermediate Stress Using a Hollow Cylinder Apparatus," Imperial College, London, 1982, pp. 1-9.

35. Yong, R.N. and McKyes, E., "Yielding of Clay in a Complex Stress Field," Proceedings of the 3rd Pan American Conference on Soil Mechanics and Foundations Engineering, Caracus, 1967, Vol. 1, pp. 131-143.

36. Yong, R.N. and Warkentin, B.P., Introduction to Soil Behavior, The Macmillan Company, New York, 1966.

APPENDIX A

TRULY TRIAXIAL TEST RESULTS

Introduction

The purpose of the experiments discussed herein was to demonstrate the use of the truly triaxial apparatus for the study of the anisotropic behavior of clay. Three undrained static tests with different orientations of the principal stress axes with respect to the know material axes were conducted.

Equipment and Experimental Procedure

Specimens

Large cylindrical samples of Georgia kaolin were prepared by K_o-consolidation of a clay slurry in a consolidometer under a normal pressure of 70 psi. When consolidation was complete, the sample was extruded from the consolidometer and left to rebound. Cubical test specimens 2 inches on a side were subsequently trimmed from the core of the consolidated sample. The clay specimens had a water content of 31%, a plastic limit of 25%, a liquid limit of 40%, and a plasticity index of 20%. The degree of saturation was 89%.

Equipment

The truly triaxial apparatus with fluid cushion boundaries designed at the University of Colorado, Boulder for multiaxial testing of cubical soil samples was used to conduct the tests. The apparatus provided capabilities for the independent application and measurement of three principal stresses in directions coincident with the axes of the apparatus. The stresses acting on the specimen were controlled manually by the operator while the corresponding deformations were monitored by a data acquisition system and then processed and recorded by a computer. The test apparatus and the operational features of the system are described in detail by Mageli (1982).

Test Procedure

The cubical test specimens were prepared in the humidity room and then transferred to the truly triaxial apparatus. The specimen was positioned on the lower face of the apparatus and the remaining five faces bolted in place. The sample cavity was saturated by generating a low gradient flow of deaired water into the cell. An open drainage port at the top edge of the cell allowed air displaced by the water to escape. After the sample cavity was fully saturated, the sample was loaded under drained conditions to a hydrostatic total stress of 5 psi and left overnight to consolidate.

The stress path followed to fail the specimens is shown in Figure 1. The applied confining stress in two directions was kept at a constant 10 psi while the stress in the third direction was increased in increments of 1 psi every 2 minutes. Deformation data was recorded for each load increment.

To simulate rotation of the principal stresses with respect to the principal material axes, the following procedure was followed. For the first test, the direction of consolidation and the major principal stress direction were coincident with the Z axis (vertical axis) of the apparatus. The angle β, the orientation of the major principal stress with respect to the axes of consolidation, was equal to 0°. For the second test, the specimen's orientation was identical to the first. The major principal stress was applied coincident with the X-axis of the apparatus and hence $\beta = 90°$. For the final test, the specimen was trimmed at an angle of 45° with respect to the direction of consolidation while maintaining the direction of one of the axes in the plane of transverse isotropy fixed. When placed in the test apparatus, the direction of consolidation was 45° with respect to the Y and Z axes and 90° to the X axis of the apparatus. The major principal stress was applied in the Z direction with β then equal to 45°.

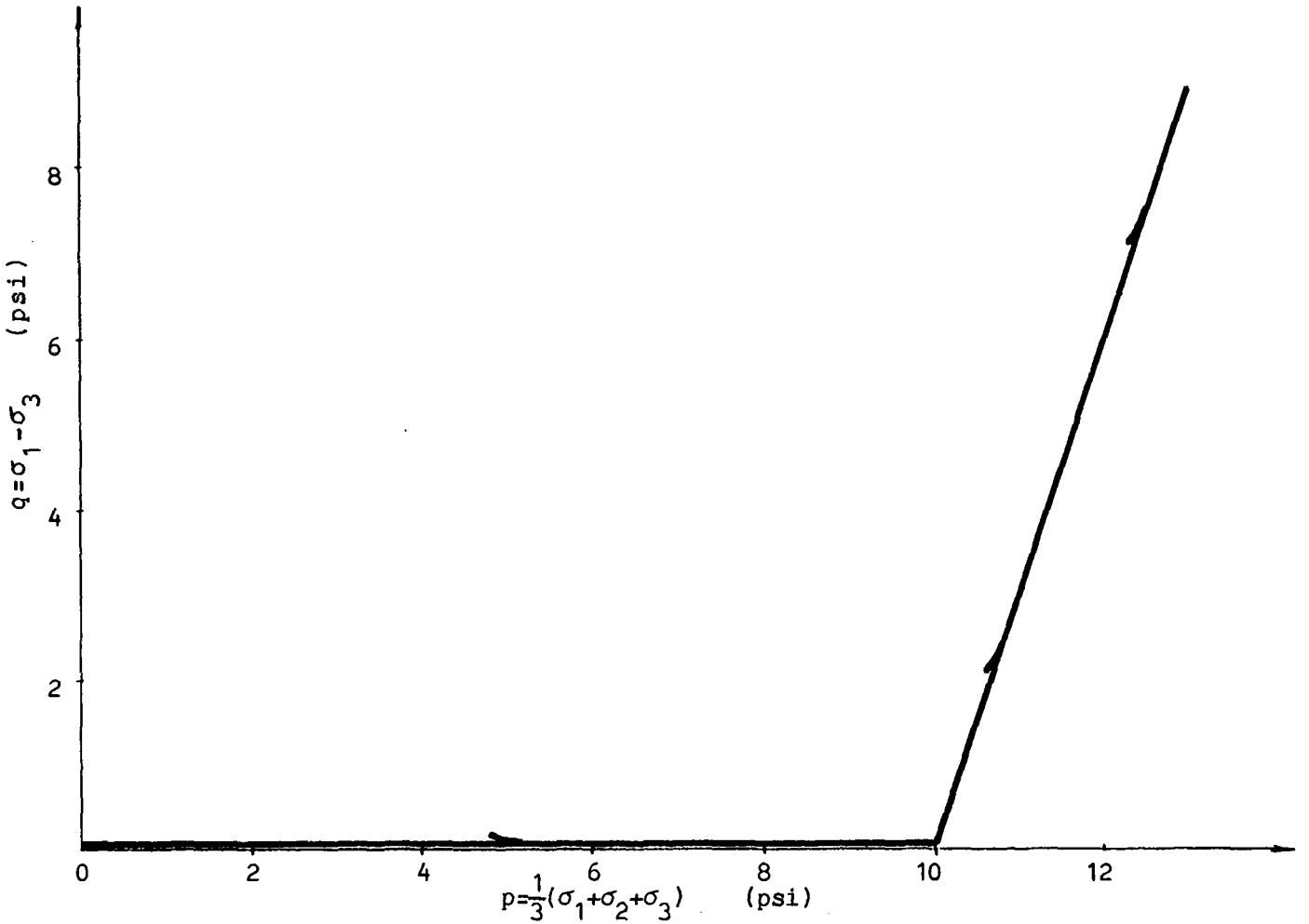

Figure 1. Stress Path to Failure

Test Results

Figures 2, 3, and 4 show the stress strain response for orientations of the major principal stress with respect to the direction of consolidation of 0°, 45°, and 90° respectively. For the sign convention used, a positive value of normal strain, ε, indicates a compressive deformation whereas a negative value indicates expansive deformation.

For the first test where $\beta = 0°$, the loading in the Z-direction resulted in axial compression and nearly equal expansion in the lateral, X and Y-directions. This response was consistent with that which is expected for a cross anisotropic specimen which is loaded normal to the plane of transverse isotropy. Accordingly, Poisson's ratio of lateral strain to axial strain in the YZ and XZ planes are identical; $\nu_{xz} = \nu_{yz} = 0.33$. Theoretically, for an undrained test the volumetric strain $\varepsilon_v = \varepsilon_x + \varepsilon_y + \varepsilon_z$, should be zero. In Figure 2, it is apparent that ε_z is consistently more than the sum of the lateral strains up to a value of $q = 9$ psi. The overall deformation of the specimen was compressive. This compression was actually the decrease in volume of air voids and is the expected response of a partially saturated soil. This overall compressive deformation was typical of all the tests.

The results of the test where $\beta = 45°$ are shown in Figure 3. Initially, the lateral strains in the X and Y-directions are more or less equal. However, after the value of q

AD-A144 872 COMPARISON OF THE HOLLOW CYLINDER AND THE TRULY TRIAXIAL TEST APPARATUSES..(U) COLORADO UNIV AT BOULDER DEPT OF CIVIL ENVIRONMENTAL AND ARCH.. F R SMITH 1983 2/2

UNCLASSIFIED N66314-70-A-0062 F/G 8/13 NL

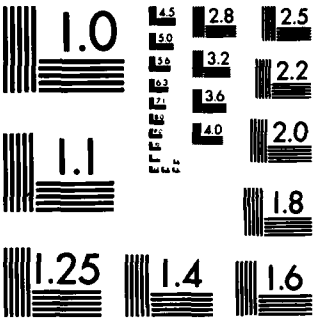

MICROCOPY RESOLUTION TEST CHART
NATIONAL BUREAU OF STANDARDS-1963-A

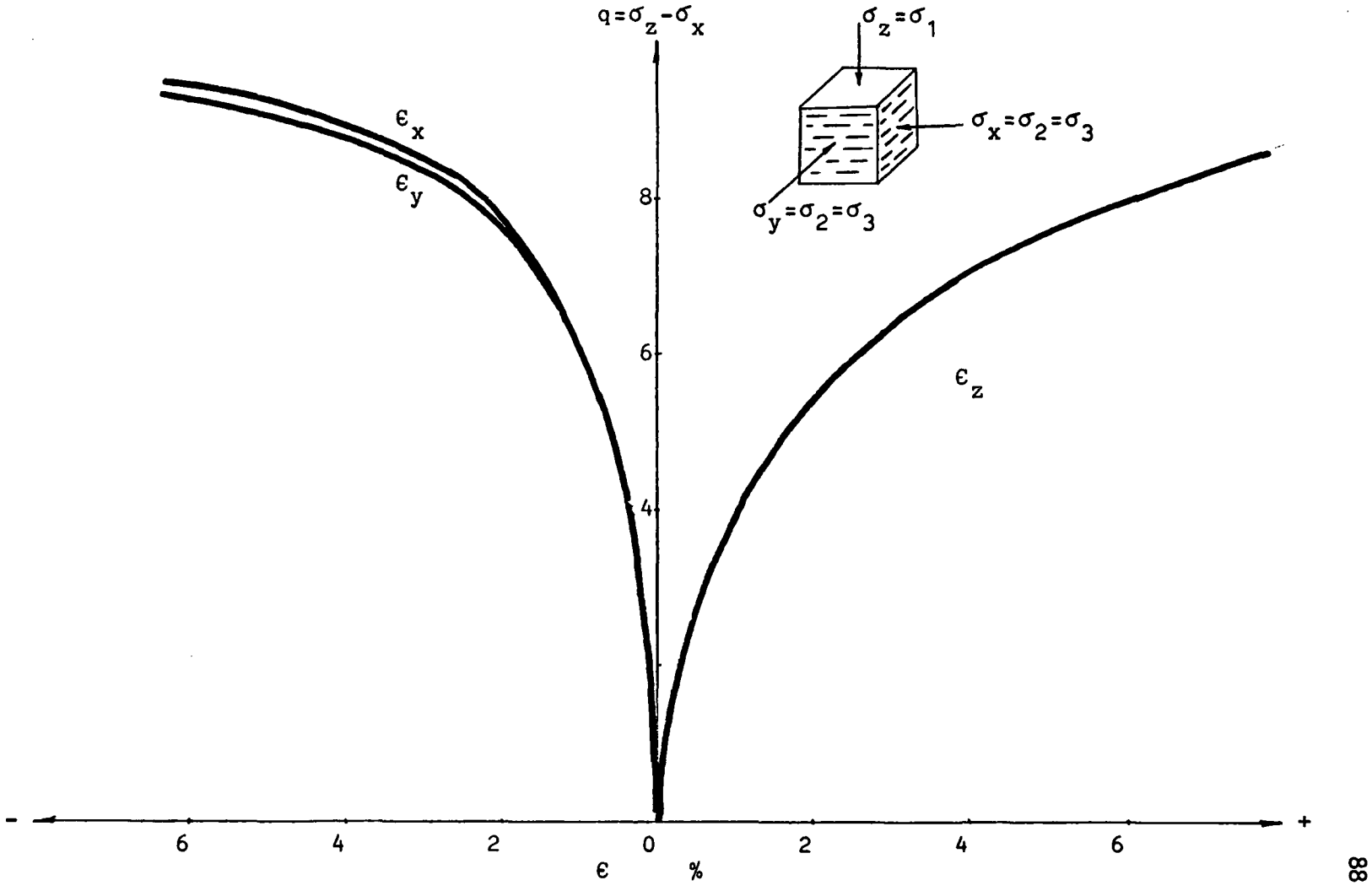

Figure 2. $\beta=0^{\circ}$

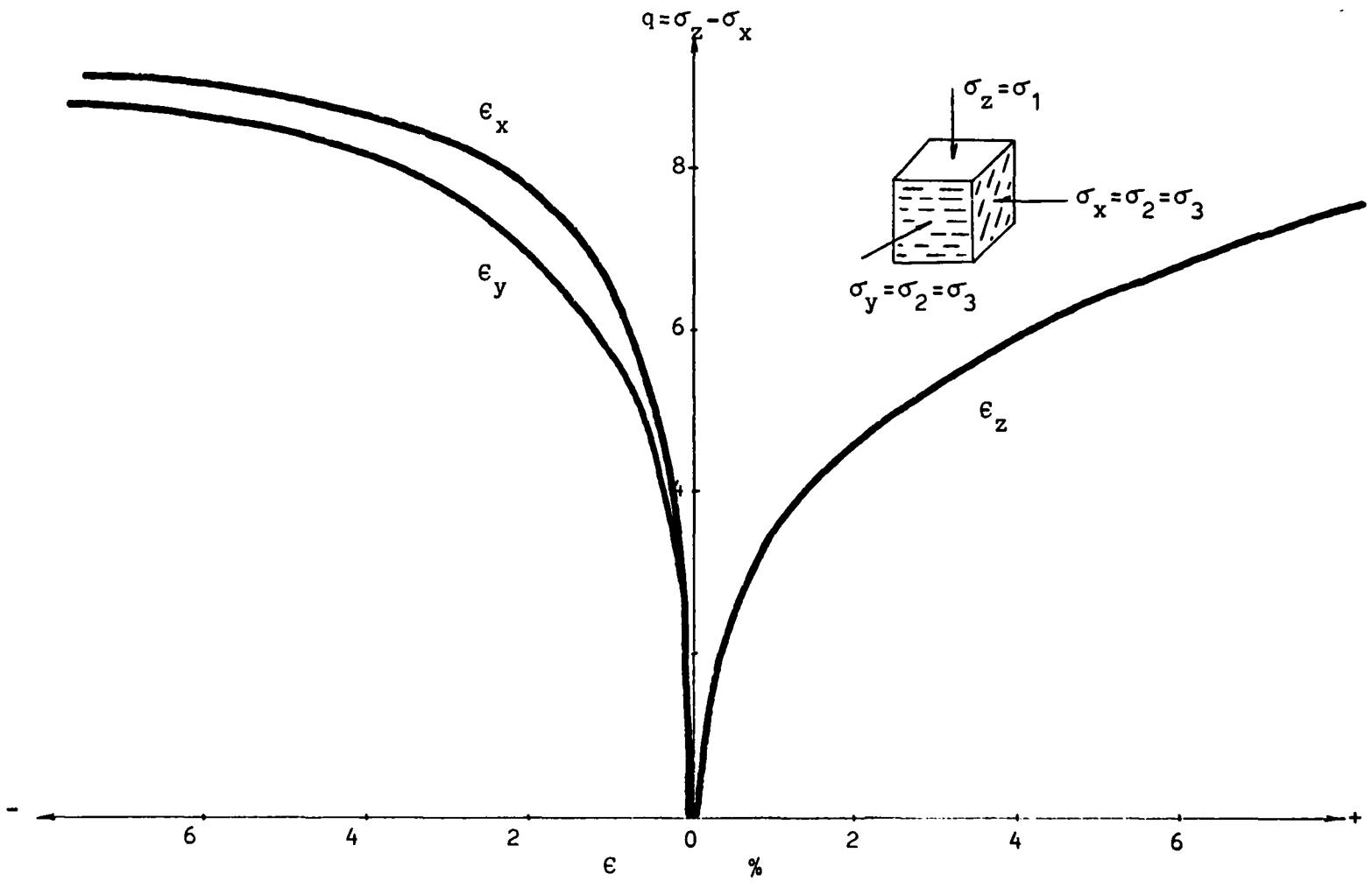

Figure 3. $\beta=45^{\circ}$

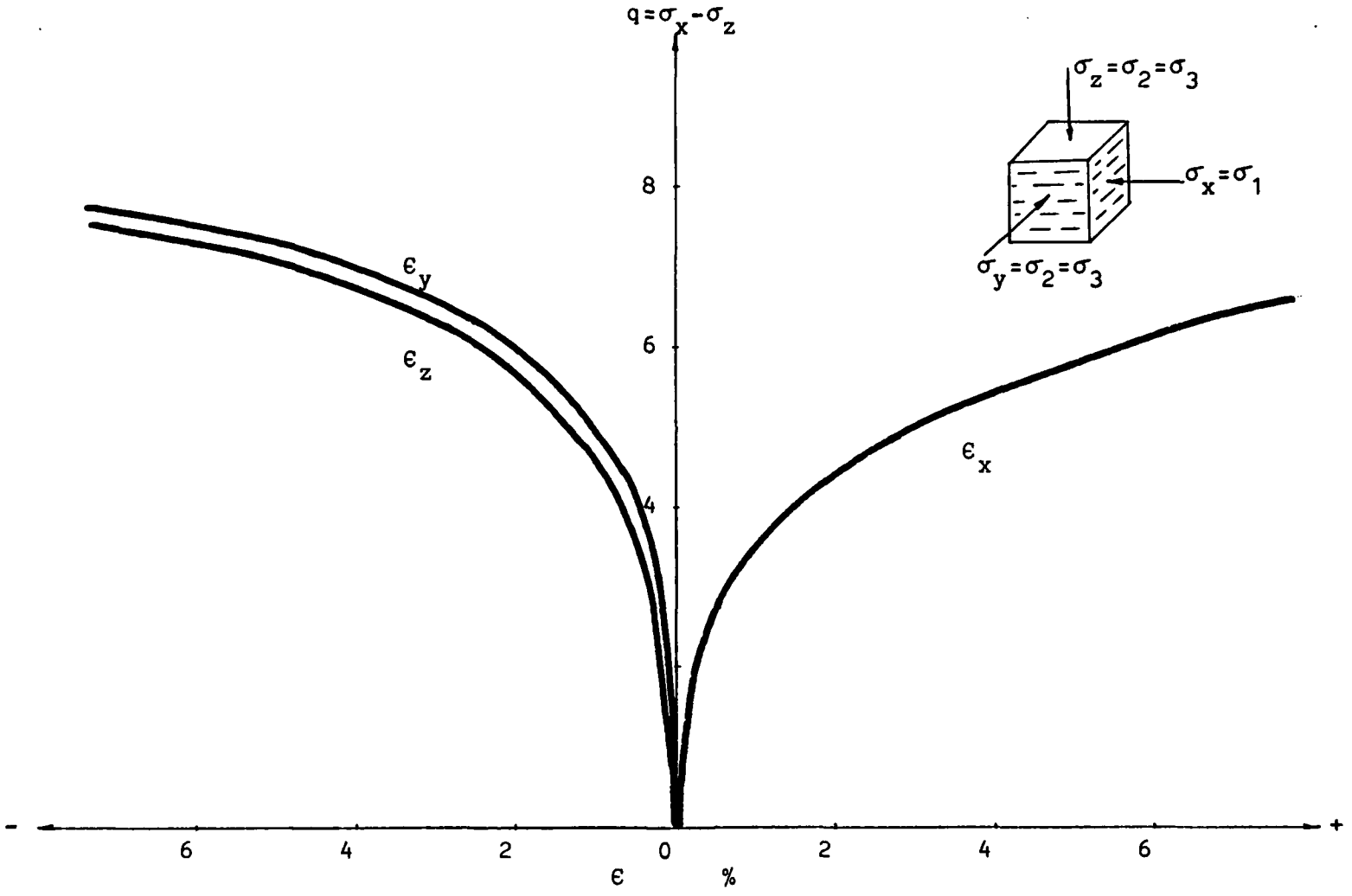

Figure 4. $\beta=90^{\circ}$

exceeds 5 psi, the principal shear plane develops and the strain in the Y-direction quickly becomes significantly greater than the strain in the X-direction.

The results of loading the specimen normal to the direction of consolidation are shown in Figure 4. For $\beta = 90°$, the response of the specimen was the least stiff. The lateral strains are unequal, the strain in the Z-direction being somewhat greater than that in the Y-direction.

Figure 5 shows the composite of all three tests plotted as shear stress versus maximum shear strain. The undrained shear strength of the cross anisotropic specimens is seen to vary with the orientation of the principal stress directions. The stiffest response and greatest strength are found when the principal stress direction and axis of consolidation are coincident, $\beta = 0°$. The least stiffness and strength are for $\beta = 90°$. Strength and stiffness of the clay specimen is due primarily to the resistance to parallel arrangement of the clay particles in the direction of shear and resistance to relative movement by sliding of clay particles over one another. The test results did show that strength was greater for shear across planes of preferred particle orientation rather than along them.

Reference

1. Mageli, T.S., "Development of a Servo-Controlled True Triaxial Cell and Cyclic Loading of Clays, M.S. Thesis, University of Colorado, 1982

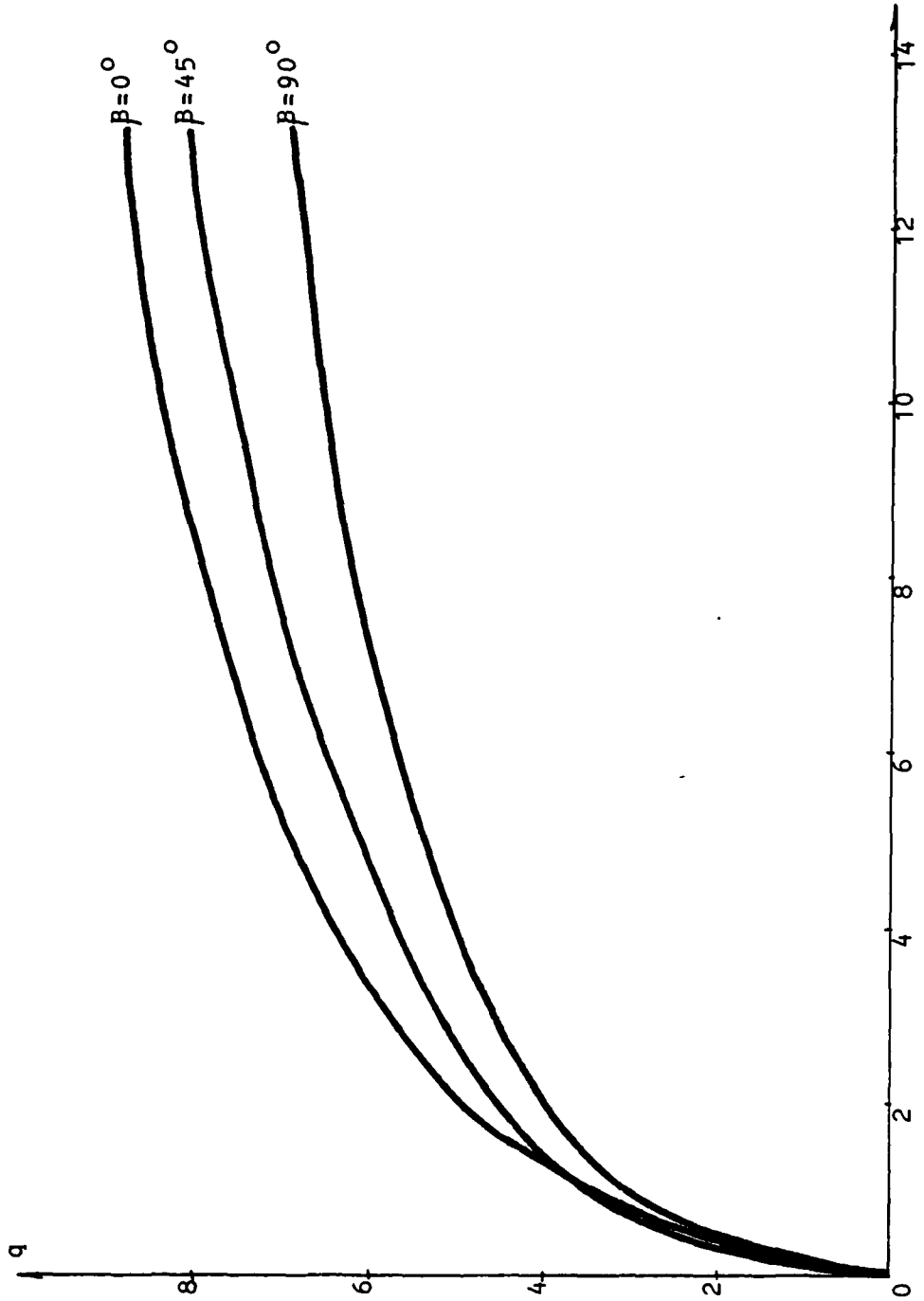

Figure 5. Results Summary

END

FILMED

9-84

DTIC